Synthesis, biological evaluation and network pharmacology based studies of 1,3,4-oxadiazole bearing azaphenols as anticancer agents

Guifen Chen [a,1], Minjie Zhang [a,1], Yafang Chen [a], Yan Zhang [a,b], Guoyong Luo [a,b], Yi Long [a,b], Wude Yang [a,b,*], Xiang Yu [a,b,*]

[a] College of Pharmacy, Guizhou University of Traditional Chinese Medicine, Guiyang 550025, China
[b] Guizhou Joint Laboratory for International Cooperation in Ethnic Medicine (Ministry of Education), Guizhou University of Traditional Chinese Medicine, Guiyang 550025, China

ABSTRACT

To discover novel and effective potential anticancer agents, a series of azophenol derivatives containing 1,3,4-oxadiazoles moiety was synthesized and investigated for their anticancer activities against several human cancer cell lines by MTT method. Their structures were characterized by ^{1}H NMR, ^{13}C NMR, IR and HRMS spectral analyses. Among the prepared compounds, **5df** displayed significant anti-proliferative activity against HCT116 cancer cells with an IC$_{50}$ value of 4.09 ± 0.04 μM. Moreover, this compound had low cytotoxicity against normal cells. Flow cytometric analysis indicated that compound **5df** arrested the cell cycle at S phase and induced apoptosis in a dose-dependent manner. Additionally, network pharmacology analysis calculated that **5df** might target several key proteins, including AKT serine/threonine kinase 1 (AKT1), SRC proto-oncogene, non-receptor tyrosine kinase (SRC). Furthermore, molecular docking study indicated that **5df** exhibited potentially high binding affinity to these target proteins with binding energies lower than −8 kcal/mol. These findings provide valuable insights for the development of azophenol derivatives as potential anticancer agents.

1. Introduction

Cancer is one of the leading causes of death in the twenty-first century and a critical challenge that needs to be addressed to increase human life expectancy (Bray et al., 2018). Recent statistics revealed a staggering 19.3 million new cancer cases and nearly ten million cancer-related deaths in 2020 (Sung et al., 2011). Colorectal cancer ranks as the third most prevalent cancer globally and the second deadliest in terms of mortality rate (Sawicki et al., 2021). The emergence and progression of colorectal cancer result from a complex interplay of factors, including age, family history, gender, geographical location, and personal medical history (Peng et al., 2018; Shen et al., 2018). Conventional treatment approaches for colorectal cancer encompass surgical intervention and chemotherapy. Chemotherapeutic agents induce DNA damage or activate diverse signaling pathways to prompt cancer cell demise, including cell cycle arrest, inhibition of global translation, blockage of DNA repair, and other mechanisms (Woods and Turchi, 2013). Hence, the discovery

and advancement of novel chemical entities that are more efficacious and less toxic would signify a groundbreaking stride in cancer research.

Azo derivatives, characterized by their nitrogen-nitrogen double bond (—N=N—), rank among the most crucial chromophores and find diverse applications in the realms of science, industry, and pharmaceuticals (Benkhaya et al., 2020; Tahir et al., 2021). Presently, the synthesis of azo derivatives has attracted significant attention due to their varied bioactivities, such as antibacterial (Atay et al., 2017), antioxidant (Mohammadi et al., 2015), antifungal (Matada et al., 2020), anti-inflammatory (Manjunatha and Bodke, 2021), and antitubercular (Manjunatha et al., 2021). Furthermore, azo derivatives also displayed substantial anticancer potentials. For example, Keshavayya et al. reported a robust anticancer heterocyclic azo derivative, dimethyl-[4-(5-methyl-thiazol-2-ylazo)-phenyl]-amine (**I,** Fig. 1), which manifested potent anticancer effects against A-549 and K-562 cell lines (Ravi et al., 2020). Another novel azo derivative, **II** (Fig. 1), exhibited notable activity against the human colon cell line (HCT116) by inhibiting the
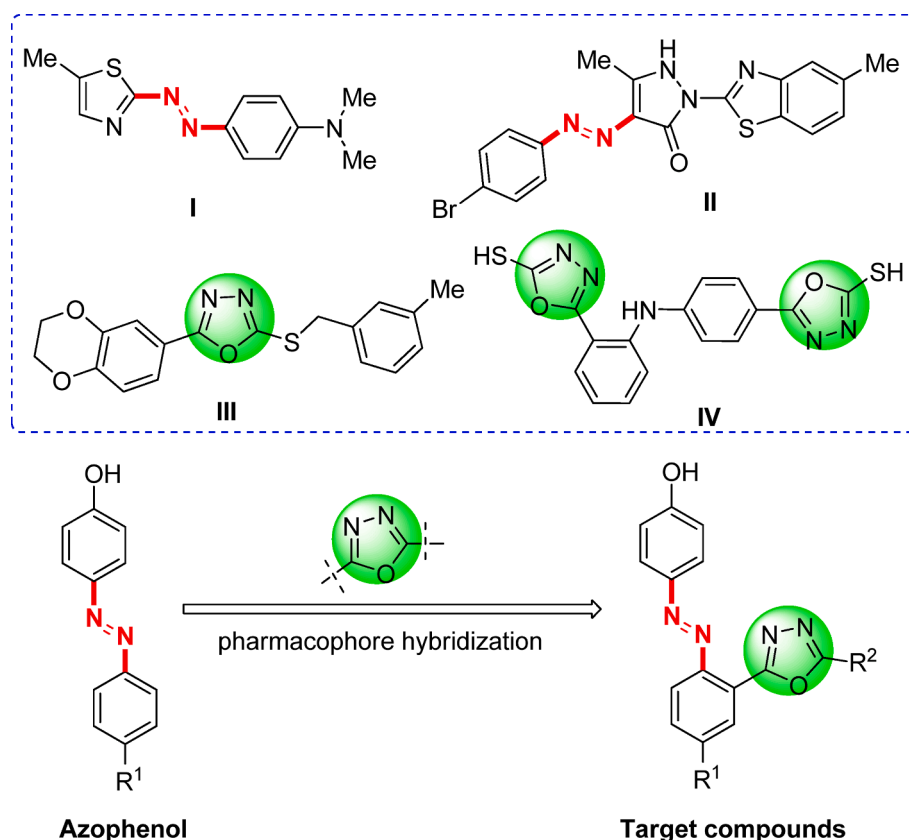
Fig. 1. Design of the azophenol derivatives containing 1,3,4-oxadiazoles moiety.

growth of the cancerous cells (Maliyappa et al., 2020).

On the other hand, 1,3,4-oxadiazole stands as a widely studied pharmacophore that has garnered significant research attention in recent years, owing to its metabolic characteristics and capacity to establish hydrogen bonds with receptor sites. These compounds serve as excellent bioisosteres of amides and esters, as the incorporation of the oxadiazole core with the azole (—N=C—O—) motif enhances lipophilicity. This property plays a pivotal role in facilitating the transmembrane diffusion of drugs, enabling them to effectively reach their intended targets (Bajaj et al., 2015; Andreani et al., 2001). These molecules exhibit diverse biological activities, including anti-inflammatory (Abd-Ellah et al., 2017), antidiabetic (Shingalapur et al., 2010), antianxiety (Harfenist et al., 1996), antifungal (Wang et al., 2021), antibacterial (Guo et al., 2019) and antitubercular etc (Ahsan et al., 2011). Notably, numerous distinct 1,3,4-oxadiazoles also displayed substantial anticancer properties against various cancer cell lines. For instance, compounds **III** and **IV** (Fig. 1) have demonstrated potent anticancer activities (Zhang et al., 2011; Abou-Seri, 2010).

The development of small molecules through molecular hybridization from known structural motifs is one of the current trends in drug discovery. It is anticipated that improved cytotoxicity may be achieved through the structural conjugation of two potent pharmacophoric units. However, there are few literature reports on the combination of azo group and 1,3,4-oxadiazole for the development of anti-tumor drug molecules. Drawing inspiration from the aforementioned facts and our prior research (Yu et al., 2021, 2023), we devised and synthesized a novel series of azophenol derivatives containing the 1,3,4-oxadiazoles moiety (Fig. 1) as potential anticancer agents. The *in vitro* anticancer activities of all target derivatives were evaluated via the MTT method against several human cancer cell lines, including lung cancer cells (A549), cervical carcinoma cells (HeLa), colon cancer cells (HCT116), hepatocellular carcinoma cells (HePG$_2$), breast cancer cells (MCF-7), HT1080 fibrosarcoma cells (HT1080). The mechanism of

antiproliferative effects of this class of compounds was studied via cell cycle arrest and cell apoptosis assay. Additionally, network pharmacology and molecular docking study were conducted to identify potential targets of these derivatives. This study may provide lead molecules for the discovery and development of anticancer candidates.

2. Experimental

2.1. Chemistry

All reagents and solvents were of reagent grade or purified according to standard methods before use. Analytical thin-layer chromatography (TLC) was performed with silica gel plates using silica gel 60 GF$_{254}$ (Qingdao Haiyang Chemical Co., Ltd., Qingdao, China). Melting points were determined on an X-5A micro melting point tester (Gongyi Kerui instrument Co., Ltd.) and were uncorrected. Infrared absorption spectra (IR) were recorded by IRTracer-100 (Shimadzu, Wikipedia, Japan). ^{1}H/^{13}C nuclear magnetic resonance (NMR) spectra were recorded on a Bruker Avance neo 400 or 600 MHz instrument (Bruker, Bremerhaven, Germany) in CDCl$_3$ or DMSO-d_6 using TMS (tetramethylsilane) as the internal standard. High-resolution mass spectrometry (HRMS) was determined by a Xevo G2-SQTOF instrument (Waters, Milford, MA, USA).

2.1.1. General procedure for the synthesis of (E)-N'-(2-nitrobenzylidene) arylhydrazides (2aa ~ eg)

To a solution of 2-nitrobenzaldehydes (**1a** ~ **e,** 1 mmol) and aryl hydrazides (1 mmol) in ethanol (EtOH, 10 mL), two drops of acetic acid (HOAc) was added, and the mixture was reflux for 1–5 h. When the reaction was complete, the mixture was cooled to room temperature until no more precipitate was observed. Then the solvent was removed under reduced pressure to give the intermediates (**2aa** ~ **eg**). The compounds were not purified and went straight to the next step.

2.1.2. General procedure for the synthesis of 2-(2-nitrophenyl)-5-aryl-1,3,4-oxadiazoles (3aa ~ eg)

The intermediates **3aa ~ eg** (1.1 mmol), K_2CO_3 (3.0 mmol, 414.6 mg) and iodine (1.1 mmol, 279.4 mg) were dissolved in dimethyl sulfoxide (DMSO, 10 mL), then the reaction mixture was stirred at 100 °C. When the reaction was complete according to TLC analysis, the mixture was treated with saturated $Na_2S_2O_3$ (20 mL) and extracted with ethyl acetate (EtOAc, 3 × 20 mL). The combined organic layer was washed with brine (3 × 20 mL), dried over anhydrous Na_2SO_4, filtered and evaporated. The given residues were purified by flash chromatography on silica gel to get the compounds **3aa ~ eg** in 61–98 % yields. Their spectral data were provided in **Supplementary Material**.

2.1.3. General procedure for the synthesis of 2-(5-aryl-1,3,4-oxadiazol-2-yl)anilines (4aa ~ eg)

A mixture of compounds **3aa ~ eg** (1 mmol), hydrated tin(II) chloride (5 mmol, 1128.5 mg) in EtOAc (10 mL) was reflux for 4-12 h. While the reaction was complete, the mixture was cooled to room temperature and adjusted to pH 8–9 with saturated $NaHCO_3$. Then the mixture was filtered and extracted with EtOAc (2 × 50 mL). The combined organic phase was washed with saturated brine (100 mL), dried over anhydrous Na_2SO_4, concentrated, and purified by flash chromatography on silica gel to obtain compounds **4aa ~ eg** in 48–93 % yields. Their spectral data were provided in **Supplementary Material**.

2.1.4. General procedure for the synthesis of (E)-4-((2-(5-aryl-1,3,4-oxadiazol-2-yl)phenyl)diazenyl) phenol derivatives (5aa ~ eg)

To a mixture of compounds **4aa ~ eg** (1 mmol), water (6 mL) and concentrated HCl (12 mol/L, 0.5 mL) at 0 °C, a solution of sodium nitrite (NaNO$_2$, 1.2 mmol) in water (6 mL) was added dropwise while maintaining the temperature below 5 °C. After stirring for 0.5–1 h, a solution of diazonium chloride was prepared. Subsequently, The solution of diazonium chloride was added gradually to a mixture of phenol (1.1 mmol), sodium hydroxide (NaOH, 2 mmol), EtOH (10 mL) and water (10 mL) at 0–5 °C. After the addition of the above diazonium solution, the mixture was continued to stir for 4–6 h until a lot of precipitate was produced. The solid was collected, washed with water (3 × 10 mL), dried and purified by flash chromatography on silica gel to afford the target products **5aa ~ eg** in 38–90 % yields. The spectroscopic and analytical data of these compounds are as follows:

2.1.4.1. (E)-4-((2-(5-phenyl-1,3,4-oxadiazol-2-yl)phenyl)diazenyl)phenol (5aa).
Yield: 48 %, Red solid, M.p.: 281–283 °C; IR cm^{-1} (KBr): 1606, 1510, 1369, 1246, 1141, 837, 704; ^{1}H NMR (400 MHz, DMSO-d_6) δ 10.50 (s, 1H), 8.20 (d, J = 7.7 Hz, 1H), 8.03 (d, J = 6.8 Hz, 2H), 7.85 – 7.78 (m, 3H), 7.74 – 7.70 (m, 2H), 7.68 – 7.59 (m, 3H), 6.95 (d, J = 8.8 Hz, 2H); ^{13}C NMR (101 MHz, DMSO-d_6) δ 164.3, 163.0, 161.2, 149.9, 145.2, 132.4, 131.7, 129.9 × 2, 129.1 × 2, 126.2 × 2, 125.1 × 2, 122.9, 120.4, 116.6, 115.6 × 2; HRMS (ESI) calcd for $C_{20}H_{14}N_4O_2Na$ ([M + Na]$^+$) 365.1008, found 365.1002.

2.1.4.2. (E)-4-((2-(5-(4-fluorophenyl)-1,3,4-oxadiazol-2-yl)phenyl)diazenyl)phenol (5ab).
Yield: 89 %, Red solid, M.p.: 273–275 °C; IR cm^{-1} (KBr): 1589, 1498, 1384, 1284, 1143, 1095, 837, 731; ^{1}H NMR (600 MHz, DMSO-d_6) δ 10.45 (s, 1H), 8.19 (dd, J = 7.6, 1.4 Hz, 1H), 8.09 – 8.07 (m, 2H), 7.82 (d, J = 8.8 Hz, 2H), 7.80 – 7.77 (m, 1H), 7.73 – 7.70 (m, 2H), 7.47 (t, J = 8.8 Hz, 2H), 6.95 (d, J = 8.8 Hz, 2H); ^{13}C NMR (101 MHz, DMSO-d_6) δ 165.4, 163.9, 163.3, 162.7, 161.6, 150.3, 145.6, 132.7, 130.3, 130.2, 129.3, 125.5 × 2, 120.8, 120.0, 117.0, 116.8, 116.6, 116.0 × 2; HRMS (ESI) calcd for $C_{20}H_{13}FN_4O_2Na$ ([M + Na]$^+$) 383.0914, found 383.0909.

2.1.4.3. (E)-4-((2-(5-(4-chlorophenyl)-1,3,4-oxadiazol-2-yl)phenyl)diazenyl)phenol (5ac).
Yield: 73 %, Red solid, M.p.: 238–239 °C; IR cm^{-1} (KBr): 1591, 1463, 1382, 1286, 1143, 835,754, 731; ^{1}H NMR (600 MHz, DMSO-d_6) δ 10.47 (s, 1H), 8.19 (dd, J = 7.8, 1.4 Hz, 1H), 8.03 (d, J = 8.5 Hz, 2H), 7.82 (d, J = 8.8 Hz, 2H), 7.78 – 7.77 (m, 1H), 7.73 – 7.67 (m, 4H), 6.96 (d, J = 8.8 Hz, 2H); ^{13}C NMR (101 MHz, DMSO-d_6) δ 163.5, 163.1, 161.2, 149.9, 145.2, 136.4, 132.4, 129.9, 129.8, 129.2 × 2, 127.9 × 2, 125.1 × 2, 121.8, 120.3, 116.6, 115.6 × 2; HRMS (ESI) calcd for $C_{20}H_{13}ClN_4O_2Na$ ([M + Na]$^+$) 399.0619, found 399.0613.

2.1.4.4. (E)-4-((2-(5-(m-tolyl)-1,3,4-oxadiazol-2-yl)phenyl)diazenyl)phenol (5ad).
Yield: 38 %, Red solid, M.p.: 214–216 °C; IR cm^{-1} (KBr): 1587, 1508, 1313, 1282, 1143, 842, 725; ^{1}H NMR (600 MHz, DMSO-d_6) δ 10.47 (s, 1H), 8.22 (dd, J = 8.0, 1.5 Hz, 1H), 7.86 (d, J = 8.8 Hz, 2H), 7.83 (d, J = 7.5 Hz, 1H), 7.79 – 7.77 (m, 2H), 7.72 – 7.69 (m, 2H), 7.49 – 7.44 (m, 2H), 6.96 (d, J = 8.8 Hz, 2H), 2.37 (s, 3H); ^{13}C NMR (101 MHz, DMSO-d_6) δ 164.8, 163.3, 161.6, 150.3, 145.6, 138.9, 132.8, 132.7, 130.2, 130.1, 129.3, 126.8, 125.5 × 2, 123.7, 123.2, 120.6, 117.0, 116.0 × 2, 20.8; HRMS (ESI) calcd for $C_{21}H_{16}N_4O_2Na$ ([M + Na]$^+$) 379.1165, found 379.1159.

2.1.4.5. (E)-4-((2-(5-(3-methoxyphenyl)-1,3,4-oxadiazol-2-yl)phenyl)diazenyl)phenol (5ae).
Yield: 89 %, Red solid, M.p.: 253–255 °C; IR cm^{-1} (KBr): 1598, 1508, 1327, 1278, 1143, 854, 731; ^{1}H NMR (400 MHz, DMSO-d_6) δ 10.50 (s, 1H), 8.21 (d, J = 8.9 Hz, 1H), 7.84 (d, J = 8.5 Hz, 2H), 7.78 (d, J = 8.9 Hz, 1H), 7.75 – 7.68 (m, 2H), 7.61 (d, J = 7.7 Hz, 1H), 7.55 – 7.46 (m, 2H), 7.22 (dd, J = 8.3, 2.7 Hz, 1H), 6.95 (d, J = 8.9 Hz, 2H), 3.80 (s, 3H); ^{13}C NMR (101 MHz, DMSO-d_6) δ 164.6, 163.4, 161.6, 159.7, 150.3, 145.6, 132.8, 130.7, 130.3, 130.2, 125.5 × 2, 124.5, 120.7, 118.8, 118.1, 117.0, 116.0 × 2, 111.2, 55.33; HRMS (ESI) calcd for $C_{21}H_{16}N_4O_3Na$ ([M + Na]$^+$) 395.1114, found 395.1105.

2.1.4.6. (E)-4-((2-(5-(benzo[d][1,3]dioxol-5-yl)-1,3,4-oxadiazol-2-yl)phenyl)diazenyl)phenol (5af).
Yield: 69 %, Red solid, M.p.: 289–291 °C; IR cm^{-1} (KBr): 1591, 1504, 1386, 1286, 1143, 837, 721; ^{1}H NMR (400 MHz, DMSO-d_6) δ 10.45 (s, 1H), 8.18 (d, J = 7.4 Hz, 1H), 7.83 (d, J = 8.7 Hz, 2H), 7.77 (t, J = 7.6 Hz, 1H), 7.71 – 7.68 (m, 2H), 7.57 (d, J = 8.1 Hz, 1H), 7.48 (s, 1H), 7.13 (d, J = 8.1 Hz, 1H), 6.95 (d, J = 8.8 Hz, 2H), 6.18 (s, 2H); ^{13}C NMR (101 MHz, DMSO-d_6) δ 164.5, 162.9, 161.6, 150.5, 150.2, 148.2, 145.6, 132.6, 130.2, 130.1, 125.5 × 2, 121.8, 120.8, 116.9, 116.0 × 2, 115.9, 109.1, 106.2, 102.1; HRMS (ESI) calcd for $C_{21}H_{14}N_4O_4Na$ ([M + Na]$^+$) 409.0907, found 409.0901.

2.1.4.7. (E)-4-((2-(5-(pyridin-4-yl)-1,3,4-oxadiazol-2-yl)phenyl)diazenyl)phenol (5ag).
Yield: 59 %, Red solid, M.p.: 250–251 °C; IR cm^{-1} (KBr): 1589, 1504, 1328, 1280, 1141, 840, 723; ^{1}H NMR (400 MHz, DMSO-d_6) δ 9.18 (d, J = 2.3 Hz, 1H), 8.82 (d, J = 4.9 Hz, 1H), 8.39 (d, J = 8.1 Hz, 1H), 8.22 (d, J = 7.6 Hz, 1H), 7.84 (d, J = 8.5 Hz, 2H), 7.79 (d, J = 7.3 Hz, 1H), 7.73 – 7.64 (m, 3H), 6.94 (d, J = 8.5 Hz, 2H); ^{13}C NMR (101 MHz, DMSO-d_6) δ 163.9, 163.2, 161.9, 152.7, 150.6, 147.4, 145.8, 134.3, 133.1, 130.5, 130.4, 125.7 × 2, 124.6, 120.7, 120.1, 117.2, 116.2 × 2; HRMS (ESI) calcd for $C_{19}H_{13}N_5O_2Na$ ([M + Na]$^+$) 366.0961, found 366.0955.

2.1.4.8. (E)-4-((4-methoxy-2-(5-phenyl-1,3,4-oxadiazol-2-yl)phenyl)diazenyl)phenol (5ba).
Yield: 55 %, Green solid, M.p.: 256–257 °C; IR cm^{-1} (KBr): 1598, 1504, 1332, 1278, 1141,831, 725; ^{1}H NMR (400 MHz, DMSO-d_6) δ 10.33 (s, 1H), 8.06 (d, J = 6.6 Hz, 2H), 7.82 (d, J = 9.0 Hz, 1H), 7.77 (d, J = 8.8 Hz, 1H), 7.70 – 7.61 (m, 4H), 7.34 (dd, J = 9.0, 2.9 Hz, 1H), 6.91 (d, J = 8.8 Hz, 2H), 3.95 (s, 3H); ^{13}C NMR (101 MHz, DMSO-d_6) δ 165.0, 163.6, 161.2, 160.8, 145.7, 144.2, 132.3, 129.7 × 2, 126.8 × 2, 125.2 × 2, 123.5, 123.4, 119.1, 118.5, 116.1 × 2, 114.4, 56.2; HRMS (ESI) calcd for $C_{21}H_{16}N_4O_3Na$ ([M + Na]$^+$) 395.1114, found 395.1107.

2.1.4.9. (E)-4-((2-(5-(4-fluorophenyl)-1,3,4-oxadiazol-2-yl)-4-methoxyphenyl)diazenyl)phenol (5bb).
Yield: 73 %, Brown solid, M.p.: 253–255 °C; IR cm^{-1} (KBr): 1597, 1496, 1328, 1278, 1141, 1091, 833, 734; ^{1}H

NMR (400 MHz, DMSO-d_6) δ 10.32 (s, 1H), 8.13 – 8.09 (m, 2H), 7.81 (d, J = 9.0 Hz, 1H), 7.75 (d, J = 8.8 Hz, 2H), 7.65 (d, J = 2.8 Hz, 1H), 7.48 (t, J = 8.8 Hz, 2H), 7.34 (dd, J = 9.0, 2.9 Hz, 1H), 6.91 (d, J = 8.8 Hz, 2H), 3.95 (s, 3H); ^{13}C NMR (101 MHz, DMSO-d_6) δ 165.6, 164.3, 163.5, 163.1, 161.2, 160.8, 145.7, 144.2, 129.5, 125.2 × 2, 123.3, 120.2, 119.0, 118.5, 117.1, 116.8, 116.1 × 2, 114.4, 56.2; HRMS (ESI) calcd for C$_{21}$H$_{15}$FN$_4$O$_3$Na ([M + Na]$^+$) 413.1020, found 413.1008.

2.1.4.10. (E)-4-((2-(5-(4-chlorophenyl)-1,3,4-oxadiazol-2-yl)-4-methoxyphenyl)diazenyl)phenol (5bc). Yield: 46 %, Red solid, M.p.: 233–235 °C; IR cm^{-1} (KBr): 1600, 1504, 1325, 1280, 1141, 833, 750, 729; ^{1}H NMR (400 MHz, DMSO-d_6) δ 10.33 (s, 1H), 8.06 (d, J = 7.7 Hz, 2H), 7.85 – 7.63 (m, 6H), 7.34 (d, J = 11.7 Hz, 1H), 6.91 (d, J = 8.4 Hz, 2H), 3.95 (s, 3H); ^{13}C NMR (101 MHz, DMSO-d_6) δ 164.3, 163.7, 161.2, 160.8, 145.7, 144.2, 137.1, 129.9 × 2, 128.6 × 2, 125.2 × 2, 123.3, 122.4, 119.1, 118.5, 116.1 × 2, 114.5, 56.2; HRMS (ESI) calcd for C$_{21}$H$_{15}$ClN$_4$O$_3$Na ([M + Na]$^+$) 429.0724, found 429.0718.

2.1.4.11. (E)-4-((4-methoxy-2-(5-(m-tolyl)-1,3,4-oxadiazol-2-yl)phenyl) diazenyl)phenol (5bd). Yield: 60 %, Brown solid, M.p.: 201–202 °C; IR cm^{-1} (KBr): 1598, 1506, 1328, 1280, 1141, 835, 725; ^{1}H NMR (400 MHz, DMSO-d_6) δ 7.91 – 7.75 (m, 5H), 7.67 (s, 1H), 7.49 (d, J = 9.0 Hz, 2H), 7.34 (d, J = 9.2 Hz, 1H), 6.91 (d, J = 8.1 Hz, 2H), 3.95 (s, 3H), 2.39 (s, 3H); ^{13}C NMR (101 MHz, DMSO-d_6) δ 165.0, 163.4, 161.1, 160.6, 145.5, 144.0, 139.0, 132.7, 129.4, 126.9, 125.0 × 2, 123.8, 123.2, 123.0, 118.9, 118.3, 115.9 × 2, 114.1, 56.0, 20.8; HRMS (ESI) calcd for C$_{22}$H$_{18}$N$_4$O$_3$Na ([M + Na]$^+$) 409.1271, found 409.1264.

2.1.4.12. (E)-4-((4-methoxy-2-(5-(3-methoxyphenyl)-1,3,4-oxadiazol-2-yl)phenyl)diazenyl)phenol (5be). Yield: 90 %, Green solid, M.p.: 202–203 °C; IR cm^{-1} (KBr): 1589, 1506, 1330, 1290, 1141, 839, 729; ^{1}H NMR (400 MHz, DMSO-d_6) δ 7.81 (d, J = 9.0 Hz, 1H), 7.76 (d, J = 8.9 Hz, 2H), 7.66 (d, J = 2.8 Hz, 1H), 7.64 (d, J = 7.9 Hz, 1H), 7.57 – 7.51 (m, 2H), 7.35 (dd, J = 9.1, 2.9 Hz, 1H), 7.23 (dd, J = 8.3, 2.7 Hz, 1H), 6.93 (d, J = 8.9 Hz, 2H), 3.95 (s, 3H), 3.82 (s, 3H); ^{13}C NMR (101 MHz, DMSO-d_6) δ 164.8, 163.5, 161.5, 160.5, 159.7, 145.4, 144.1, 130.8, 125.0 × 2, 124.5, 123.0, 119.1, 118.9, 118.4, 118.2, 116.1 × 2, 114.2, 111.4, 56.0, 55.4; HRMS (ESI) calcd for C$_{22}$H$_{18}$N$_4$O$_4$Na ([M + Na]$^+$) 425.1220, found 425.1209.

2.1.4.13. (E)-4-((2-(5-(benzo[d][1,3]dioxol-5-yl)-1,3,4-oxadiazol-2-yl)-4-methoxyphenyl)diazenyl)phenol (5bf). Yield: 61 %, Brown solid, M.p.: 271–272 °C; IR cm^{-1} (KBr): 1589, 1502, 1325, 1288, 1141, 837, 731; ^{1}H NMR (400 MHz, DMSO-d_6) δ 10.42 (s, 1H), 7.80 – 7.74 (m, 3H), 7.64 – 7.57 (m, 2H), 7.52 (d, J = 1.8 Hz, 1H), 7.33 (dd, J = 9.0, 2.9 Hz, 1H), 7.14 (d, J = 8.1 Hz, 1H), 6.93 (d, J = 8.9 Hz, 2H), 6.19 (s, 2H), 3.95 (s, 3H); ^{13}C NMR (101 MHz, DMSO-d_6) δ 164.6, 162.9, 161.1, 160.6, 150.5, 148.2, 145.5, 143.9, 125.0 × 2, 123.2, 121.9, 118.8, 118.3, 116.9, 115.9 × 2, 114.1, 109.2, 106.3, 102.2, 56.0; HRMS (ESI) calcd for C$_{22}$H$_{16}$N$_4$O$_5$Na ([M + Na]$^+$) 439.1012, found 439.1010.

2.1.4.14. (E)-4-((4-methoxy-2-(5-(pyridin-4-yl)-1,3,4-oxadiazol-2-yl) phenyl)diazenyl)phenol (5bg). Yield: 45 %, Red solid, M.p.: 288–289 °C; IR cm^{-1} (KBr): 1597, 1504, 1336, 1280, 1141, 839, 725; ^{1}H NMR (400 MHz, DMSO-d_6) δ 10.43 (s, 1H), 9.22 (s, 1H), 8.84 (s, 1H), 8.42 (d, J = 7.5 Hz, 1H), 7.82 – 7.75 (m, 3H), 7.68 (s, 2H), 7.35 (d, J = 8.8 Hz, 1H), 6.92 (d, J = 8.8 Hz, 2H), 3.96 (s, 3H); ^{13}C NMR (101 MHz, DMSO-d_6) δ 163.7, 163.1, 161.1, 160.5, 152.6, 147.3, 145.5, 144.0, 134.2, 125.0 × 2, 124.4, 122.8, 119.9, 119.0, 118.4, 115.9 × 2, 114.2, 56.0; HRMS (ESI) calcd for C$_{20}$H$_{15}$N$_5$O$_3$Na ([M + Na]$^+$) 396.1067, found 396.1056.

2.1.4.15. (E)-4-((4-ethoxy-2-(5-phenyl-1,3,4-oxadiazol-2-yl)phenyl)dia-zenyl)phenol (5ca). Yield: 76 %, Green solid, M.p.: 242–244 °C; IR cm^{-1} (KBr): 1597, 1477, 1332, 1240, 1141, 833, 725; ^{1}H NMR (400 MHz, DMSO-d_6) δ 10.36 (s, 1H), 8.06 (d, J = 6.8 Hz, 2H), 7.78 – 7.75 (m, 3H),

7.72 – 7.60 (m, 4H), 7.32 (dd, J = 9.0, 2.8 Hz, 1H), 6.91 (d, J = 8.4 Hz, 2H), 4.22 (q, J = 7.0 Hz, 2H), 1.41 (t, J = 6.9 Hz, 3H); ^{13}C NMR (101 MHz, DMSO-d_6) δ 164.8, 163.4, 161.0, 159.9, 145.6, 143.9, 132.2, 129.5 × 2, 126.6 × 2, 125.0 × 2, 123.3, 123.2, 119.2, 118.4, 115.9 × 2, 114.7, 64.1, 14.5; HRMS (ESI) calcd for C$_{22}$H$_{18}$N$_4$O$_3$Na ([M + Na]$^+$) 409.1271, found 409.1263.

2.1.4.16. (E)-4-((4-ethoxy-2-(5-(4-fluorophenyl)-1,3,4-oxadiazol-2-yl) phenyl)diazenyl)phenol (5cb). Yield: 74 %, Red solid, M.p.: 281–283 °C; IR cm^{-1} (KBr): 1595 1496, 1328, 1278, 1141, 1093, 833, 734; ^{1}H NMR (400 MHz, DMSO-d_6) δ 8.13 – 8.10 (m, 2H), 7.81 (d, J = 9.0 Hz, 1H), 7.74 (d, J = 8.8 Hz, 2H), 7.63 (d, J = 2.8 Hz, 1H), 7.48 (t, J = 8.9 Hz, 2H), 7.33 (dd, J = 9.0, 2.8 Hz, 1H), 6.89 (d, J = 8.8 Hz, 2H), 4.23 (q, J = 6.9 Hz, 2H), 1.41 (t, J = 6.9 Hz, 3H); ^{13}C NMR (101 MHz, DMSO-d_6) δ 165.4, 164.0, 163.3, 162.9, 161.4, 159.8, 145.3, 143.9, 129.3, 125.0 × 2, 123.1, 120.0, 119.1, 118.3, 116.9, 116.6, 116.0 × 2, 114.7, 64.1, 14.5; HRMS (ESI) calcd for C$_{22}$H$_{17}$FN$_4$O$_3$Na ([M + Na]$^+$) 427.1176, found 427.1165.

2.1.4.17. (E)-4-((2-(5-(4-chlorophenyl)-1,3,4-oxadiazol-2-yl)-4-ethoxyphenyl)diazenyl)phenol (5 cc). Yield: 81 %, Brown solid, M.p.: 260–262 °C; IR cm^{-1} (KBr): 1600, 1483, 1327, 1278, 1141, 833, 750, 729; ^{1}H NMR (400 MHz, DMSO-d_6) δ 10.31 (s, 1H), 8.06 (d, J = 8.6 Hz, 2H), 7.80 (d, J = 9.0 Hz, 1H), 7.75 (d, J = 8.8 Hz, 2H), 7.70 (d, J = 8.6 Hz, 2H), 7.63 (d, J = 2.9 Hz, 1H), 7.32 (dd, J = 9.1, 2.8 Hz, 1H), 6.91 (d, J = 8.8 Hz, 2H), 4.22 (q, J = 7.0 Hz, 2H), 1.40 (t, J = 6.9 Hz, 3H); ^{13}C NMR (101 MHz, DMSO-d_6) δ 164.0, 163.4, 161.0, 159.9, 145.5, 143.8, 136.8, 129.6 × 2, 128.3 × 2, 125.0 × 2, 123.0, 122.2, 119.2, 118.3, 115.9 × 2, 114.7, 64.1, 14.5. HRMS (ESI) calcd for C$_{22}$H$_{17}$ClN$_4$O$_3$Na ([M + Na]$^+$) 443.0881, found 443.0873.

2.1.4.18. (E)-4-((4-ethoxy-2-(5-(m-tolyl)-1,3,4-oxadiazol-2-yl)phenyl) diazenyl)phenol (5 cd). Yield: 63 %, Green solid, M.p.: 220–222 °C; IR cm^{-1} (KBr): 1597, 1506, 1325, 1278, 1143, 833, 684; ^{1}H NMR (400 MHz, DMSO-d_6) δ 10.33 (s, 1H), 7.87 – 7.82 (m, 2H), 7.79 – 7.76 (m, 3H), 7.64 (d, J = 2.8 Hz, 1H), 7.53 – 7.45 (m, 2H), 7.31 (dd, J = 9.1, 2.8 Hz, 1H), 6.91 (d, J = 8.8 Hz, 2H), 4.22 (q, J = 7.0 Hz, 2H), 2.39 (s, 3H), 1.41 (t, J = 6.9 Hz, 3H); ^{13}C NMR (101 MHz, DMSO-d_6) δ 164.9, 163.3, 161.0, 159.8, 145.5, 143.8, 138.9, 132.7, 129.3, 126.9, 125.0 × 2, 123.7, 123.2, 123.0, 119.1, 118.3, 115.9 × 2, 114.5, 64.0, 20.8, 14.5; HRMS (ESI) calcd for C$_{23}$H$_{20}$N$_4$O$_3$Na ([M + Na]$^+$) 423.1427, found 423.1417.

2.1.4.19. (E)-4-((4-ethoxy-2-(5-(3-methoxyphenyl)-1,3,4-oxadiazol-2-yl) phenyl)diazenyl)phenol (5ce). Yield: 82 %, Red solid, M.p.: 230–232 °C; IR cm^{-1} (KBr): 1598, 1467, 1325, 1278, 1141, 833, 729; ^{1}H NMR (400 MHz, DMSO-d_6) δ 10.33 (s, 1H), 7.78 (t, J = 8.4 Hz, 3H), 7.68 – 7.60 (m, 2H), 7.55 – 7.49 (m, 2H), 7.31 (dd, J = 9.1, 2.8 Hz, 1H), 7.23 (d, J = 8.2 Hz, 1H), 6.91 (d, J = 8.5 Hz, 2H), 4.22 (q, J = 6.9 Hz, 2H), 3.82 (s, 3H), 1.40 (t, J = 7.0 Hz, 3H); ^{13}C NMR (101 MHz, DMSO-d_6) δ 164.7, 163.4, 161.0, 159.9, 159.7, 145.5, 143.9, 130.7, 125.0 × 2, 124.5, 123.1, 119.1, 118.9, 118.3, 118.1, 115.9 × 2, 114.6, 111.3, 64.1, 55.3, 14.5. HRMS (ESI) calcd for C$_{23}$H$_{20}$N$_4$O$_4$Na ([M + Na]$^+$) 439.1376, found 439.1364.

2.1.4.20. (E)-4-((2-(5-(benzo[d][1,3]dioxol-5-yl)-1,3,4-oxadiazol-2-yl)-4-ethoxyphenyl)diazenyl)phenol (5cf). Yield: 71 %, Red solid, M.p.: 251–253 °C; IR cm^{-1} (KBr): 1597 1502, 1323, 1278, 1141, 833, 731; ^{1}H NMR (400 MHz, DMSO-d_6) δ 10.32 (s, 1H), 7.77 (t, J = 8.6 Hz, 3H), 7.64 – 7.57 (m, 2H), 7.52 (s, 1H), 7.30 (dd, J = 9.0, 2.8 Hz, 1H), 7.14 (d, J = 8.1 Hz, 1H), 6.91 (d, J = 8.8 Hz, 2H), 6.18 (s, 2H), 4.21 (q, J = 7.0 Hz, 2H), 1.40 (t, J = 6.9 Hz, 3H); ^{13}C NMR (101 MHz, DMSO-d_6) δ 164.5, 162.9, 160.9, 159.9, 150.5, 148.1, 145.5, 143.8, 125.0 × 2, 123.2, 121.8, 119.0, 118.2, 116.9, 115.9 × 2, 114.9, 109.1, 106.2, 102.1, 64.0, 14.5. HRMS (ESI) calcd for C$_{23}$H$_{18}$N$_4$O$_5$Na ([M + Na]$^+$) 453.1169,

found 453.1163.

2.1.4.21. (E)-4-((4-ethoxy-2-(5-(pyridin-4-yl)-1,3,4-oxadiazol-2-yl)phenyl)diazenyl)phenol (5cg). Yield: 74 %, Red solid, M.p.: 269–271 ℃; IR cm^{-1} (KBr): 1598 1504, 1338, 1280, 1143, 833, 727; ^{1}H NMR (400 MHz, DMSO-d_6) δ 10.32 (s, 1H), 9.23 (s, 1H), 8.83 (d, J = 3.7 Hz, 1H), 8.42 (d, J = 8.1 Hz, 1H), 7.78 – 7.75 (m, 3H), 7.68 – 7.61 (m, 2H), 7.33 (dd, J = 9.0, 2.9 Hz, 1H), 6.91 (d, J = 8.9 Hz, 2H), 4.23 (q, J = 6.9 Hz, 2H), 1.41 (t, J = 6.9 Hz, 3H); ^{13}C NMkR (101 MHz, DMSO-d_6) δ 163.6, 163.0, 161.0, 159.8, 152.6, 147.3, 145.5, 143.9, 134.2, 125.0 × 2, 124.4, 122.8, 119.9, 119.2, 118.3, 115.9 × 2, 114.7, 64.1, 14.4; HRMS (ESI) calcd for C$_{21}$H$_{17}$N$_5$O$_3$Na ([M + Na]$^+$) 410.1223, found 410.1213.

2.1.4.22. (E)-4-((2-(5-phenyl-1,3,4-oxadiazol-2-yl)-4-propoxyphenyl)diazenyl)phenol (5da). Yield: 82 %, Red solid, M.p.: 247–248 ℃; IR cm^{-1} (KBr): 1598, 1467, 1330, 1236, 1141, 844, 721; ^{1}H NMR (400 MHz, DMSO-d_6) δ 10.34 (s, 1H), 8.06 (d, J = 7.3 Hz, 2H), 7.81 – 7.75 (m, 3H), 7.69 – 7.59 (m, 4H), 7.32 (d, J = 6.2 Hz, 1H), 6.92 (d, J = 8.4 Hz, 2H), 4.11 (t, J = 6.6 Hz, 2H), 1.80 (h, J = 7.1 Hz, 2H), 1.03 (t, J = 7.4 Hz, 3H); ^{13}C NMR (101 MHz, DMSO-d_6) δ 164.6, 163.1, 160.8, 159.2, 145.3, 143.6, 131.9, 129.2 × 2, 126.4 × 2, 124.8 × 2, 123.1, 123.0, 118.9, 118.0, 115.7, 115.6, 114.5, 69.6, 21.7, 10.1; HRMS (ESI) calcd for C$_{23}$H$_{20}$N$_4$O$_3$Na ([M + Na]$^+$) 423.1427, found 423.1419.

2.1.4.23. (E)-4-((2-(5-(4-fluorophenyl)-1,3,4-oxadiazol-2-yl)-4-propoxyphenyl)diazenyl)phenol (5db). Yield: 74 %, Green solid, M.p.: 235–236 ℃; IR cm^{-1} (KBr): 1597 1496, 1328, 1278, 1141, 1093, 839, 734; ^{1}H NMR (400 MHz, DMSO-d_6) δ 10.33 (s, 1H), 8.11 (s, 2H), 7.80 – 7.773 (m, 3H), 7.62 (s, 1H), 7.48 (t, J = 8.6 Hz, 2H), 7.31 (d, J = 9.2 Hz, 1H), 6.92 (d, J = 8.5 Hz, 2H), 4.10 (t, J = 6.4 Hz, 2H), 1.81 (p, J = 6.8 Hz, 2H), 1.03 (t, J = 7.4 Hz, 3H); ^{13}C NMR (101 MHz, DMSO-d_6) δ 165.6, 164.2, 163.5, 163.1, 161.1, 160.2, 145.7, 144.0, 129.5, 125.1 × 2, 123.3, 120.2, 119.2, 118.4, 117.0, 116.7, 116.1 × 2, 114.9, 70.0, 22.0, 10.4. HRMS (ESI) calcd for C$_{23}$H$_{19}$FN$_4$O$_3$Na ([M + Na]$^+$) 441.1333, found 441.1327.

2.1.4.24. (E)-4-((2-(5-(4-chlorophenyl)-1,3,4-oxadiazol-2-yl)-4-propoxyphenyl)diazenyl)phenol (5dc). Yield: 64 %, Red solid, M.p.: 209–210 ℃; IR cm^{-1} (KBr): 1600, 1483, 1328, 1284, 1141, 833, 752, 731; ^{1}H NMR (400 MHz, DMSO-d_6) δ 8.05 (d, J = 8.6 Hz, 2H), 7.79 (d, J = 9.0 Hz, 1H), 7.75 (d, J = 8.9 Hz, 2H), 7.69 (d, J = 8.6 Hz, 2H), 7.62 (d, J = 2.8 Hz, 1H), 7.31 (dd, J = 9.0, 2.8 Hz, 1H), 6.93 (d, J = 8.8 Hz, 2H), 4.10 (t, J = 6.5 Hz, 2H), 1.80 (q, J = 7.0 Hz, 2H), 1.03 (t, J = 7.4 Hz, 3H); ^{13}C NMR (101 MHz, DMSO-d_6) δ 164.0, 163.5, 161.0, 160.0, 145.5, 143.9, 136.8, 129.6 × 2, 128.3 × 2, 124.9 × 2, 123.0, 122.2, 119.1, 118.3, 115.9 × 2, 114.7, 69.8, 21.9, 10.2. HRMS (ESI) calcd for C$_{23}$H$_{19}$ClN$_4$O$_3$Na ([M + Na]$^+$) 457.1037, found 457.1030.

2.1.4.25. (E)-4-((4-propoxy-2-(5-(m-tolyl)-1,3,4-oxadiazol-2-yl)phenyl)diazenyl)phenol (5dd). Yield: 59 %, Red solid, M.p.: 214–216 ℃; IR cm^{-1} (KBr): 1598, 1506, 1328, 1280, 1141, 842, 727; ^{1}H NMR (400 MHz, DMSO-d_6) δ 10.34 (s, 1H), 7.89 – 7.82 (m, 2H), 7.78 (d, J = 8.8 Hz, 3H), 7.65 (d, J = 2.8 Hz, 1H), 7.53 – 7.43 (m, 2H), 7.32 (dd, J = 9.0, 2.8 Hz, 1H), 6.92 (d, J = 8.5 Hz, 2H), 4.11 (t, J = 6.6 Hz, 2H), 2.39 (s, 3H), 1.80 (q, J = 7.0 Hz, 2H), 1.03 (t, J = 7.4 Hz, 3H); ^{13}C NMR (101 MHz, DMSO-d_6) δ 164.9, 163.3, 160.9, 160.0, 145.5, 143.8, 138.9, 132.6, 129.3, 126.8, 124.9 × 2, 123.7, 123.2, 123.0, 119.1, 118.3, 115.8 × 2, 114.5, 69.8, 21.8, 20.7, 10.2. HRMS (ESI) calcd for C$_{24}$H$_{22}$N$_4$O$_3$Na ([M + Na]$^+$) 437.1584, found 437.1575.

2.1.4.26. (E)-4-((2-(5-(3-methoxyphenyl)-1,3,4-oxadiazol-2-yl)-4-propoxyphenyl)diazenyl)phenol (5de). Yield: 73 %, Red solid, M.p.: 198–199 ℃; IR cm^{-1} (KBr): 1595, 1465, 1330, 1273, 1145, 842, 731; ^{1}H NMR (400 MHz, DMSO-d_6) δ 10.35 (s, 1H), 7.79 – 7.74 (m, 3H), 7.64 – 7.61 (m, 2H), 7.55 – 7.50 (m, 2H), 7.31 (dd, J = 9.1, 2.8 Hz, 1H), 7.23 (dd, J = 8.3, 1.6 Hz, 1H), 6.91 (d, J = 8.8 Hz, 2H), 4.11 (t, J = 6.5 Hz, 2H), 3.82 (s, 3H), 1.80 (q, J = 7.0 Hz, 2H), 1.03 (t, J = 7.4 Hz, 3H); ^{13}C NMR (101 MHz, DMSO-d_6) δ 165.1, 163.8, 161.4, 160.4, 160.1, 145.9, 144.3, 131.1, 125.3 × 2, 124.9, 123.4, 119.5, 119.2, 118.7, 118.4, 116.3 × 2, 115.1, 111.7, 70.2, 55.7, 22.3, 10.6. HRMS (ESI) calcd for C$_{24}$H$_{22}$N$_4$O$_4$Na ([M + Na]$^+$) 453.1533, found 453.1524.

2.1.4.27. (E)-4-((2-(5-(benzo[d][1,3]dioxol-5-yl)-1,3,4-oxadiazol-2-yl)-4-propoxyphenyl)diazenyl)phenol (5df). Yield: 77 %, Green solid, M.p.: 251–252 ℃; IR cm^{-1} (KBr): 1598 1502, 1384, 1280, 1141, 842, 731; ^{1}H NMR (400 MHz, DMSO-d_6) δ 10.37 (s, 1H), 7.78 – 7.74 (m, 3H), 7.63 – 7.56 (m, 2H), 7.53 (s, 1H), 7.32 (dd, J = 9.0, 2.9 Hz, 1H), 7.15 (d, J = 8.1 Hz, 1H), 6.91 (d, J = 8.9 Hz, 2H), 6.18 (s, 2H), 4.12 (t, J = 6.5 Hz, 2H), 1.80 (h, J = 6.9 Hz, 2H), 1.03 (t, J = 7.4 Hz, 3H); ^{13}C NMR (101 MHz, DMSO-d_6) δ 165.1, 163.5, 161.6, 160.6, 151.1, 148.8, 146.1, 144.4, 125.5 × 2, 123.8, 122.4, 119.6, 118.9, 117.6, 116.5 × 2, 115.2, 109.7, 106.8, 102.7, 70.4, 22.5, 10.8. HRMS (ESI) calcd for C$_{24}$H$_{20}$N$_4$O$_5$Na ([M + Na]$^+$) 467.1325, found 467.1320.

2.1.4.28. (E)-4-((4-propoxy-2-(5-(pyridin-4-yl)-1,3,4-oxadiazol-2-yl)phenyl)diazenyl)phenol (5dg). Yield: 52 %, Red solid, M.p.: 237–238 ℃; IR cm^{-1} (KBr): 1597 1504, 1384, 1282, 1139, 840, 725; ^{1}H NMR (400 MHz, DMSO-d_6) δ 10.48 (s, 1H), 9.25 (d, J = 2.2 Hz, 1H), 8.86 (d, J = 4.9 Hz, 1H), 8.48 (d, J = 8.1 Hz, 1H), 7.80 – 7.71 (m, 4H), 7.66 (d, J = 2.8 Hz, 1H), 7.33 (dd, J = 9.0, 2.8 Hz, 1H), 6.94 (d, J = 8.9 Hz, 2H), 4.12 (t, J = 6.5 Hz, 2H), 1.81 (p, J = 7.1 Hz, 2H), 1.03 (t, J = 7.4 Hz, 3H); ^{13}C NMR (101 MHz, DMSO-d_6) δ 163.5, 162.6, 160.9, 159.8, 151.7, 146.5, 145.3, 143.7, 134.6, 124.7 × 2, 124.4, 122.5, 119.9, 119.0, 118.1, 115.7 × 2, 114.6, 69.6, 21.6, 10.0. HRMS (ESI) calcd for C$_{22}$H$_{19}$N$_5$O$_3$Na ([M + Na]$^+$) 424.1380, found 424.1371.

2.1.4.29. (E)-4-((4-(allyloxy)-2-(5-phenyl-1,3,4-oxadiazol-2-yl)phenyl)diazenyl)phenol (5ea). Yield: 65 %, Green solid, M.p.: 238–239 ℃; IR cm^{-1} (KBr): 1597, 1504, 1330, 1276, 1240, 1141, 835, 727; ^{1}H NMR (400 MHz, DMSO-d_6) δ 10.33 (s, 1H), 8.07 (d, J = 6.9 Hz, 2H), 7.81 (d, J = 9.0 Hz, 1H), 7.77 (d, J = 8.8 Hz, 2H), 7.70 – 7.61 (m, 4H), 7.36 (d, J = 9.1 Hz, 1H), 6.91 (d, J = 8.8 Hz, 2H), 6.16 – 6.06 (m, 1H), 5.48 (d, J = 17.3 Hz, 1H), 5.34 (d, J = 10.5 Hz, 1H), 4.78 (d, J = 5.1 Hz, 2H); ^{13}C NMR (101 MHz, DMSO-d_6) δ 165.3, 163.8, 161.5, 159.9, 146.0, 144.5, 133.5, 132.6, 129.9 × 2, 127.0 × 2, 125.5 × 2, 123.8, 123.6, 119.8, 118.8, 118.5, 116.4 × 2, 115.5, 69.4; HRMS (ESI) calcd for C$_{23}$H$_{18}$N$_4$O$_3$Na ([M + Na]$^+$) 421.1271, found 421.1263.

2.1.4.30. (E)-4-((4-(allyloxy)-2-(5-(4-fluorophenyl)-1,3,4-oxadiazol-2-yl)phenyl)diazenyl)phenol (5eb). Yield: 87 %, Green solid, M.p.: 236–237 ℃; IR cm^{-1} (KBr): 1595, 1496, 1328, 1278, 1141, 1093, 837, 734; ^{1}H NMR (400 MHz, DMSO-d_6) δ 10.34 (s, 1H), 8.13 – 8.10 (m, 2H), 7.80 (d, J = 9.0 Hz, 1H), 7.76 (d, J = 8.8 Hz, 2H), 7.67 (d, J = 2.6 Hz, 1H), 7.48 (t, J = 8.8 Hz, 2H), 7.36 (d, J = 9.0 Hz, 1H), 6.92 (d, J = 8.8 Hz, 2H), 6.16 – 6.06 (m, 1H), 5.49 (d, J = 17.3 Hz, 1H), 5.34 (d, J = 10.5 Hz, 1H), 4.78 (d, J = 5.2 Hz, 2H); ^{13}C NMR (101 MHz, DMSO-d_6) δ 165.9, 164.5, 163.7, 161.5, 159.9, 146.0, 144.5, 133.4, 129.8, 129.7, 125.5 × 2, 123.5, 120.4, 119.8, 118.7, 118.5, 117.3, 117.1, 116.4 × 2, 115.5, 69.4; HRMS (ESI) calcd for C$_{23}$H$_{17}$FN$_4$O$_3$Na ([M + Na]$^+$) 439.1176, found 439.1171.

2.1.4.31. (E)-4-((4-(allyloxy)-2-(5-(4-chlorophenyl)-1,3,4-oxadiazol-2-yl)phenyl)diazenyl)phenol (5ec). Yield: 50 %, Brown solid, M.p.: 241–243 ℃; IR cm^{-1} (KBr): 1589, 1506, 1328, 1282, 1141, 833, 750, 729; ^{1}H NMR (400 MHz, DMSO-d_6) δ 10.53 (s, 1H), 8.06 (d, J = 8.4 Hz, 2H), 7.80 (d, J = 9.0 Hz, 1H), 7.75 (d, J = 8.6 Hz, 2H), 7.71 (d, J = 8.4 Hz, 2H), 7.67 (d, J = 2.2 Hz, 1H), 7.36 (d, J = 9.0 Hz, 1H), 6.96 (d, J = 8.7 Hz, 2H), 6.18 – 6.04 (m, 1H), 5.49 (d, J = 17.4 Hz, 1H), 5.34 (d, J = 10.5 Hz, 1H), 4.78 (d, J = 4.6 Hz, 2H); ^{13}C NMR (101 MHz, DMSO-d_6) δ 164.5, 163.9, 161.7, 159.9, 145.9, 144.5, 137.3, 133.4, 130.1 × 2,
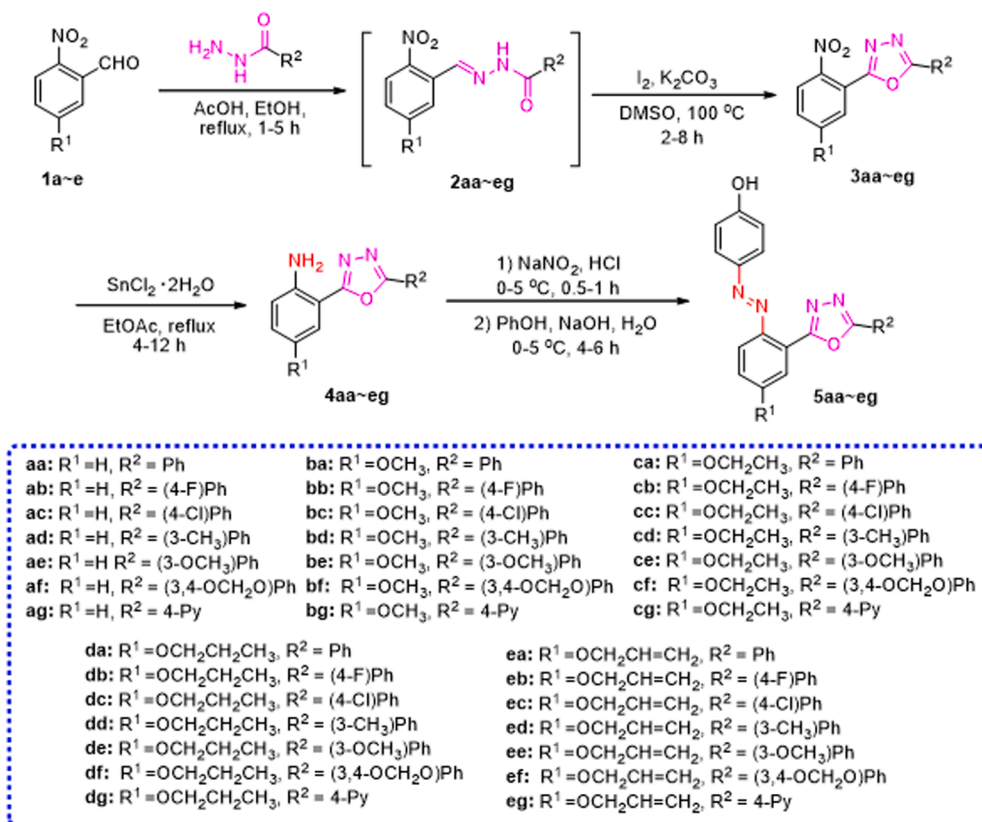
Scheme 1. General synthetic procedure of azophenol derivatives containing 1,3,4-oxadiazoles moiety (**5aa ~ eg**).

Table 1
The structure, yield, and melting point of all target compounds.

Compound	R^1	R^2	Yield (%)	M.p. (°C)
5aa	H	Ph	48	281–283
5ab	H	(4-F)Ph	89	273–275
5ac	H	(4-Cl)Ph	73	238–239
5ad	H	(3-CH₃)Ph	38	214–216
5ae	H	(3-OCH₃)Ph	89	253–255
5af	H	(3,4-OCH₂O)Ph	69	289–291
5ag	H	4-Py	59	250–251
5ba	OCH₃	Ph	55	256–257
5bb	OCH₃	(4-F)Ph	73	253–255
5bc	OCH₃	(4-Cl)Ph	46	233–235
5bd	OCH₃	(3-CH₃)Ph	60	201–202
5be	OCH₃	(3-OCH₃)Ph	90	202–203
5bf	OCH₃	(3,4-OCH₂O)Ph	61	271–272
5bg	OCH₃	4-Py	45	288–289
5ca	OCH₂CH₃	Ph	76	242–244
5cb	OCH₂CH₃	(4-F)Ph	74	281–283
5cc	OCH₂CH₃	(4-Cl)Ph	81	260–262
5cd	OCH₂CH₃	(3-CH₃)Ph	63	220–222
5ce	OCH₂CH₃	(3-OCH₃)Ph	82	230–232
5cf	OCH₂CH₃	(3,4-OCH₂O)Ph	71	251–253
5cg	OCH₂CH₃	4-Py	74	269–271
5da	OCH₂CH₂CH₃	Ph	82	247–248
5db	OCH₂CH₂CH₃	(4-F)Ph	74	235–236
5dc	OCH₂CH₂CH₃	(4-Cl)Ph	64	209–210
5dd	OCH₂CH₂CH₃	(3-CH₃)Ph	59	214–216
5de	OCH₂CH₂CH₃	(3-OCH₃)Ph	73	198–199
5df	OCH₂CH₂CH₃	(3,4-OCH₂O)Ph	77	251–252
5dg	OCH₂CH₂CH₃	4-Py	52	237–238
5ea	OCH₂CH = CH₂	Ph	65	238–239
5eb	OCH₂CH = CH₂	(4-F)Ph	87	236–237
5ec	OCH₂CH = CH₂	(4-Cl)Ph	50	241–243
5ed	OCH₂CH = CH₂	(3-CH₃)Ph	86	213–214
5ee	OCH₂CH = CH₂	(3-OCH₃)Ph	54	186–187
5ef	OCH₂CH = CH₂	(3,4-OCH₂O)Ph	68	245–247
5eg	OCH₂CH = CH₂	4-Py	70	230–232

128.8 × 2, 125.4 × 2, 123.4, 122.6, 119.9, 118.8, 118.5, 116.4 × 2, 115.5, 69.41; HRMS (ESI) calcd for $C_{23}H_{17}ClN_4O_3Na$ ([M + Na]$^+$) 455.0881, found 455.0874.

2.1.4.32. (E)-4-((4-(allyloxy)-2-(5-(m-tolyl)-1,3,4-oxadiazol-2-yl) phenyl)diazenyl)phenol (5ed). Yield: 86 %, Red solid, M.p.: 213–214 °C; IR cm^{-1} (KBr): 1597, 1506, 1327, 1278, 1141, 842, 727; ^{1}H NMR (400 MHz, DMSO-d_6) δ 10.36 (s, 1H), 7.88 – 7.76 (m, 5H), 7.69 (d, J = 2.7 Hz, 1H), 7.53 – 7.46 (m, 2H), 7.35 (dd, J = 9.0, 2.8 Hz, 1H), 6.92 (d, J = 8.8 Hz, 2H), 6.19 – 6.05 (m, 1H), 5.49 (dd, J = 17.3, 1.7 Hz, 1H), 5.34 (dd, J = 10.6, 1.8 Hz, 1H), 4.78 (d, J = 4.9 Hz, 2H), 2.39 (s, 3H); ^{13}C NMR (101 MHz, DMSO-d_6) δ 164.9, 163.3, 161.1, 159.5, 145.6, 144.0, 138.9, 133.0, 132.7, 129.3, 126.9, 125.0 × 2, 123.8, 123.2, 123.0, 119.4, 118.3, 118.0, 115.9 × 2, 114.9, 68.9, 20.8. HRMS (ESI) calcd for $C_{24}H_{20}N_4O_3N$ ([M + Na]$^+$) 435.1427, found 435.1420.

2.1.4.33. (E)-4-((4-(allyloxy)-2-(5-(3-methoxyphenyl)-1,3,4-oxadiazol-2-yl)phenyl)diazenyl)phenol (5ee). Yield: 54 %, Red solid, M.p.: 186–187 °C; IR cm^{-1} (KBr): 1598, 1506, 1325, 1278, 1141, 837, 729; ^{1}H NMR (400 MHz, DMSO-d_6) δ 10.34 (s, 1H), 7.79 (t, J = 9.3 Hz, 3H), 7.70 – 7.62 (m, 2H), 7.57 – 7.50 (m, 2H), 7.36 (dd, J = 9.0, 2.9 Hz, 1H), 7.23 (dd, J = 8.2, 2.7 Hz, 1H), 6.91 (d, J = 8.4 Hz, 2H), 6.19 – 6.05 (m, 1H), 5.49 (d, J = 17.3 Hz, 1H), 5.34 (d, J = 10.6 Hz, 1H), 4.78 (d, J = 5.2 Hz, 2H), 3.82 (s, 3H); ^{13}C NMR (101 MHz, DMSO-d_6) δ 165.3, 164.0, 161.5, 160.3, 160.1, 146.2, 144.7, 133.6, 131.4, 125.6 × 2, 125.1, 123.6, 120.0, 119.5, 119.0, 118.8, 118.7, 116.5 × 2, 115.6, 112.0, 69.5, 55.9. HRMS (ESI) calcd for $C_{24}H_{20}N_4O_4Na$ ([M + Na]$^+$) 451.1376, found 451.1369.

2.1.4.34. (E)-4-((4-(allyloxy)-2-(5-(benzo[d][1,3]dioxol-5-yl)-1,3,4-oxadiazol-2-yl)phenyl)diazenyl)phenol (5ef). Yield: 68 %, Brown solid, M.p.: 245–247 °C; IR cm^{-1} (KBr): 1597, 1502, 1458, 1323, 1280, 1141, 835, 731; ^{1}H NMR (400 MHz, DMSO-d_6) δ 10.33 (s, 1H), 7.78 (t, J = 8.8

Table 2

The anticancer activities of target compounds **5aa ~ eg** against six human cancer cells at 200 μmol/L.

Compound	Growth Inhibition Rate (%)[a]					
	A549	HeLa	HCT116	HePG2	MCF-7	HT1080
5aa	NA[b]	NA	NA	42.95 ± 2.14	NA	NA
5ab	NA	48.68 ± 5.23	13.58 ± 4.46	70.65 ± 1.38	33.92 ± 6.35	NA
5ac	NA	NA	52.93 ± 7.12	40.93 ± 3.09	NA	NA
5ad	14.74 ± 4.77	31.15 ± 4.6	33 ± 5.13	79.03 ± 3.57		NA
5ae	NA	43.51 ± 8.65	51.48 ± 2.66	67.95 ± 3.58	NA	NA
5af	NA	NA	28.99 ± 2.96	54.34 ± 3.1	NA	NA
5ag	16.51 ± 6.66	3.66 ± 30.35	14.78 ± 3.12	55.55 ± 3.99	NA	NA
5ba	NA	NA	35.7 ± 3.03	41.06 ± 2.88	NA	24.62 ± 1.62
5bb	NA	NA	17.31 ± 4.67	17.5 ± 6.29	13.51 ± 4.94	38.74 ± 3.47
5bc	19.15 ± 4.28	32.4 ± 5.1	75.9 ± 3.42	35.54 ± 5.84	NA	NA
5bd	–	NA	NA	40 ± 4.3	NA	44.17 ± 7.21
5be	13.41 ± 2.33	39.82 ± 4.11	79.71 ± 0.37	73.11 ± 3.36	NA	NA
5bf	NA	18.38 ± 2.55	NA	59.67 ± 5.65	NA	34.15 ± 0.14
5bg	NA	NA	NA	55.72 ± 5.02	47.86 ± 2.99	18.74 ± 2.87
5ca	51.96 ± 2.67	NA	35.5 ± 5.92	60.69 ± 3.29	NA	NA
5cb	NA	NA	65.22 ± 1.04	69.22 ± 4.16	NA	NA
5cc	45.69 ± 0.37	83.7 ± 2.34	62.66 ± 3.94	42 ± 5.84	58.52 ± 4.6	18.69 ± 3.16
5cd	NA	NA	22.29 ± 3.14	39.95 ± 5.51	9.04 ± 4.29	NA
5ce	NA	NA	23.38 ± 6.7	84.57 ± 3.19	28.25 ± 3.77	NA
5cf	NA	NA	7.24 ± 4.65	42.05 ± 4.48	NA	23.93 ± 6.05
5cg	12.42 ± 2.64	67.37 ± 5.11	12.58 ± 1.59	23.11 ± 2.47	10.13 ± 2.64	6.81 ± 1.76
5da	33.56 ± 5.71	27.72 ± 5.08	48 ± 2.28	83.85 ± 5.15	18.49 ± 5.43	NA
5db	NA	85.81 ± 1.26	85.41 ± 2.35	78.24 ± 2.01	49.24 ± 2.78	6.81 ± 1.76
5dc	NA	88.68 ± 1.39	62.39 ± 5.71	88.24 ± 2.01	NA	NA
5dd	NA	14.05 ± 4.84	46.51 ± 2.11	87.08 ± 2.39	44.5 ± 3	NA
5de	NA	59.43 ± 6.2	53.91 ± 2.04	53.55 ± 5.42	NA	45.35 ± 5.2
5df	62.09 ± 4.68	78.87 ± 3.78	92.47 ± 3.5	73.66 ± 5.79	64.22 ± 0.94	54.23 ± 1.94
5dg	NA	27.97 ± 8.79	26.95 ± 3.78	78.72 ± 3.32	NA	18.14 ± 2.83
5ea	NA	6.07 ± 15.84	7.63 ± 5.3	44.62 ± 5.6	NA	7.91 ± 1.11
5eb	NA	NA	36.93 ± 2.22	43.53 ± 4.97	26.18 ± 4.18	38.09 ± 5.78
5ec	40.9 ± 4.76	80.13 ± 1.58	65.03 ± 3.51	81.13 ± 7.22	28.74 ± 3.64	24.6 ± 7.42
5ed	NA	20.96 ± 5.82	36.75 ± 4.74	55.64 ± 5.34	21.08 ± 8.97	35.06 ± 6.57
5ee	NA	NA	30.62 ± 2.63	62.64 ± 4.96	10.03 ± 7.33	NA
5ef	NA	NA	41.56 ± 0.64	56.18 ± 5.23	31.93 ± 5.4	NA
5eg	53.9 ± 1.02	50.16 ± 2.47	70.52 ± 1.31	87.69 ± 0.11	38.81 ± 4.15	21.06 ± 2.16
5-FU	81.16 ± 2.95	83.74 ± 2.93	92.36 ± 3.64	88.02 ± 3.21	88.84 ± 1.26	69.01 ± 3.90

[a] The values given are means of three experiments.

[b] NA means no action.

Table 3

IC$_{50}$ values of target compounds against selected human cancer cells.

Compound	IC$_{50}$ (μM)[a]		
	HeLa	HCT116	HePG2
5ab	ND[b]	ND	>100
5ad	ND	ND	>100
5bc	ND	>100	ND
5be	ND	40.56 ± 0.45	29.6 ± 0.73
5cc	>100	ND	ND
5ce	ND	ND	>100
5da	ND	ND	13.7 ± 0.72
5db	70.77 ± 0.73	9.96 ± 0.08	44.64 ± 0.59
5dc	24.97 ± 0.16	ND	9.39 ± 0.45
5dd	ND	ND	38.43 ± 0.69
5dg	ND	ND	>100
5df	>100	4.09 ± 0.04	>100
5ec	21.79 ± 0.35	ND	36.77 ± 0.51
5eg	ND	61.69 ± 0.77	>100
5-FU	51.65 ± 0.78	2.20 ± 0.13	32.56 ± 0.64

[a] The values given are means of three experiments.
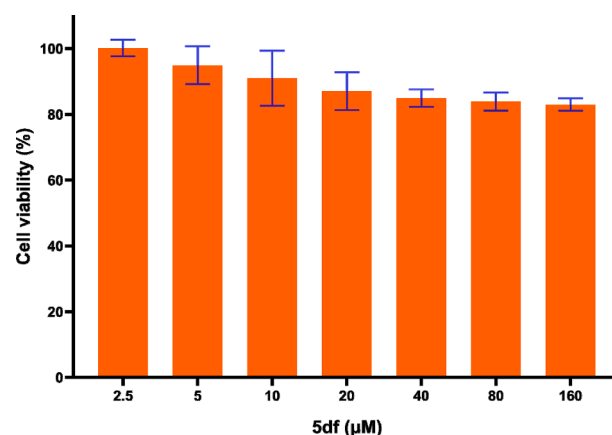
[b] ND means no detection.

Fig. 2. Relative cell viabilities of BEAS-2B treated with compound **5df**.

Hz, 3H), 7.67 (d, J = 2.9 Hz, 1H), 7.60 (dd, J = 8.1, 1.8 Hz, 1H), 7.52 (d, J = 1.7 Hz, 1H), 7.34 (dd, J = 9.0, 2.9 Hz, 1H), 7.14 (d, J = 8.1 Hz, 1H), 6.92 (dd, J = 8.9, 2.4 Hz, 2H), 6.18 (s, 2H), 6.14 – 6.06 (m, 1H), 5.48 (dd, J = 17.3, 1.7 Hz, 1H), 5.34 (dd, J = 10.5, 1.6 Hz, 1H), 4.77 (d, J = 5.2 Hz, 2H); ^{13}C NMR (101 MHz, DMSO-d_6) δ 164.6, 162.8, 161.0, 159.5, 150.5, 148.2, 145.6, 144.0, 133.0, 125.0 × 2, 123.1, 121.9, 119.3, 118.3, 118.0, 116.9, 115.9, 115.8, 114.9, 109.2, 106.3, 102.1, 68.9. HRMS (ESI) calcd for $C_{24}H_{18}N_4O_5Na$ ([M + Na]$^+$) 465.1169, found 465.1166.

2.1.4.35.   (E)-4-((4-(allyloxy)-2-(5-(pyridin-4-yl)-1,3,4-oxadiazol-2-yl) phenyl)diazenyl)phenol (5eg). Yield: 70 %, Red solid, M.p.: 230–232 ℃; IR cm^{-1} (KBr): 1597, 1506, 1321, 1278, 1141, 835, 725; ^{1}H NMR (400 MHz, DMSO-d_6) δ 9.22 (s, 1H), 8.83 (d, J = 3.2 Hz, 1H), 8.42 (d, J = 8.0 Hz, 1H), 7.80 (d, J = 9.0 Hz, 1H), 7.75 (d, J = 8.6 Hz, 2H), 7.71 – 7.63 (m, 2H), 7.36 (dd, J = 9.0, 2.8 Hz, 1H), 6.88 (d, J = 8.4 Hz, 2H), 6.17 – 6.05 (m, 1H), 5.49 (d, J = 19.3 Hz, 1H), 5.34 (d, J = 9.4 Hz, 1H), 4.78 (d, J = 5.2 Hz, 2H); ^{13}C NMR (101 MHz, DMSO-d_6) δ 163.9, 163.2, 162.3, 159.5, 152.8, 147.5, 145.2, 144.4, 134.4, 133.2, 125.4 × 2, 124.6, 122.8, 120.1, 119.7, 118.6, 118.3, 116.4 × 2, 115.2, 69.1; HRMS (ESI) calcd for $C_{22}H_{17}N_5O_3Na$ ([M + Na]$^+$) 422.1223, found 422.1215.
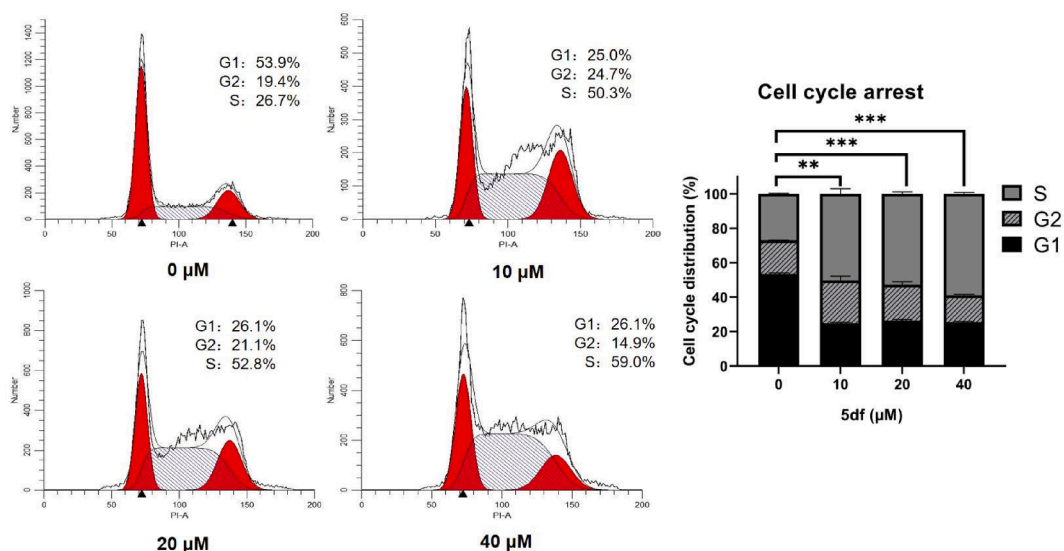
Fig. 3. Effect of compound **5df** on cell cycle in HCT116 cells. Flow cytometry of HCT116 cells treated with **5df** for 48 h (** $p < 0.01$; *** $p < 0.001$).
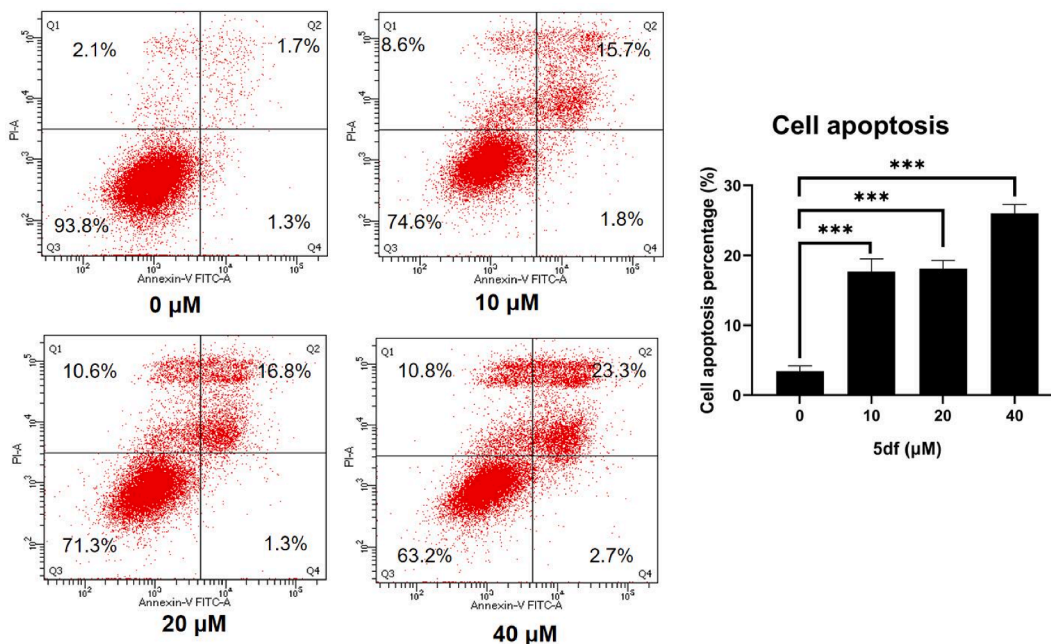

Fig. 4. Effect of compound **5df** on cell apoptosis in HCT116 cells. Flow cytometric analysis of apoptotic cells after treatment of HCT116 cells with **5df** for 48 h (*** $p < 0.001$).

2.2. Biology assays

2.2.1. Cell line and culture conditions

The human lung cancer cells (A549), human cervical carcinoma cells (HeLa), human colon cancer cells (HCT116), human hepatocellular carcinoma cell (HePG$_2$), human breast cancer cells (MCF-7), HT1080 human fibrosarcoma cells (HT1080), human lung epithelial cells (BEAS-2B) were obtained from Cell Bank/Stem Cell Bank, Chinese Academy of Sciences. We used RPMI-1640 and DMEM medium supplemented with 10 % fetal bovine serum and 1 % penicillin for cell growth under the condition of 37 °C in 5 % CO$_2$. 5- Fluorouracil (5-FU) was employed as positive control drug.

2.2.2. Cytotoxic assays

The MTT assay was used to evaluate the cytotoxicity of novel synthesized derivatives (**5aa** ~ **eg**) on cell viability. When cells were in exponentially growing phase, seeded at a concentration of 10,000 cells/well on 96 tissue culture plate overnight. After the culture medium replaced with a fresh one, a solution of synthesized compounds in DMSO was added to reach the concentration of 200 μmol/L. After 72 h, the drug solutions discarded and cells were washed with PBS. Then 3-(4,5-dimethylthiazol-2-yl)-2,5-diphenyltetrazolium bromide (MTT) (5 mg/mL, in PBS) was added into each well and cultured for another 4 h. Subsequently, the supernatant replaced with DMSO to soften the formed formazan. In parallel, we used negative control, blank and positive control (5-fluorouracil, **5-FU**) in the same conditions. At the final step, absorbance at the wavelength of 490 nm was read by a microplate reader. the IC$_{50}$ values for some compounds were also calculated. All the experiments were repeated three times.
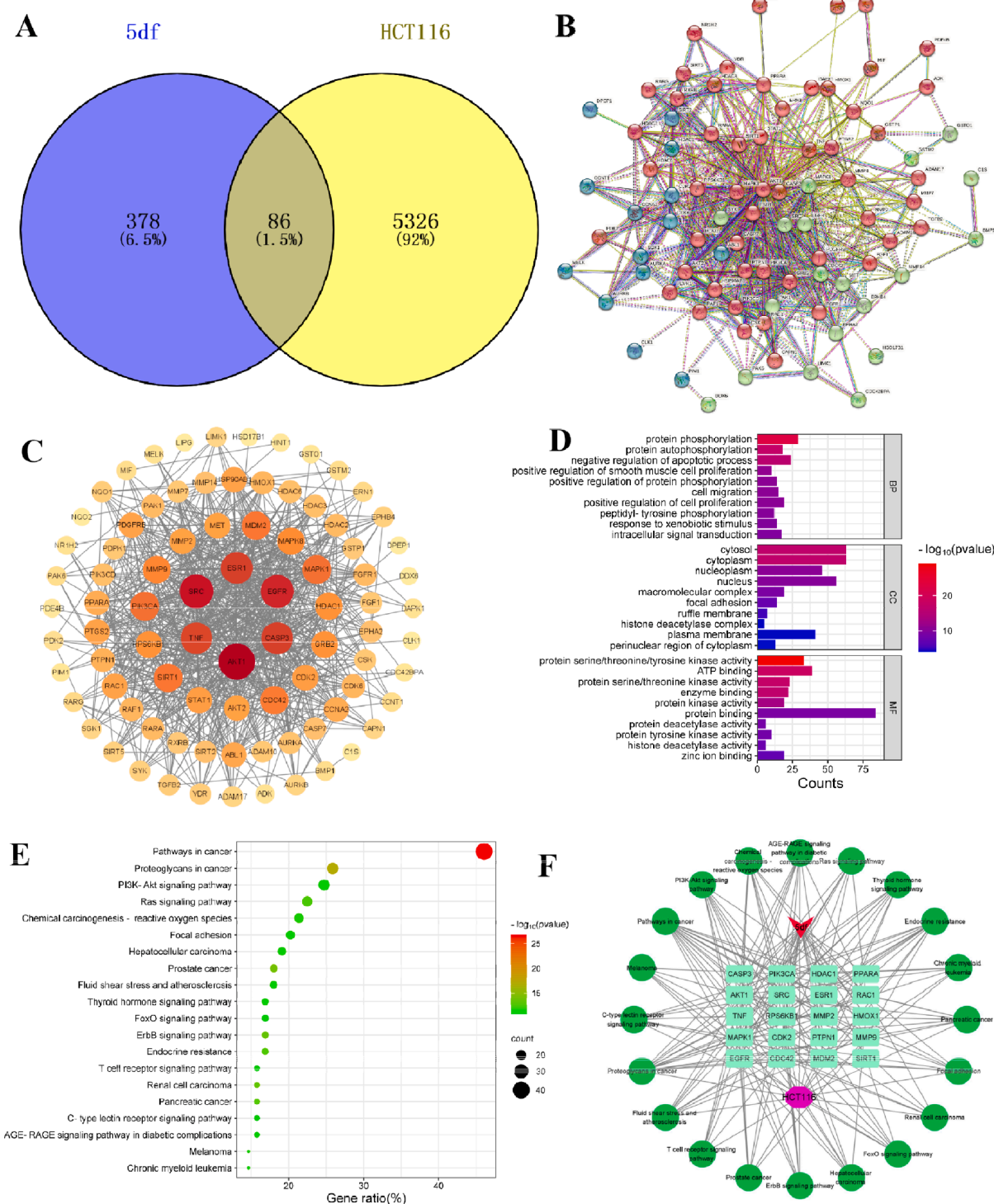
Fig. 5. Analysis of network pharmacology of **5df**-HCT116. (**A**) The Venn diagram of compound **5df** and HCT116 targets; (**B**) Protein-protein interaction (PPI) network; (**C**) Topological network schematic of proteins targeted by **5df** and associated with HCT116; (**D**) Analysis of potential targets of **5df** for anti-HCT116 based on GO enrichment; (**E**) Analysis of potential targets of **5df** for anti-HCT116 based on KEGG enrichment; (**F**) Constituent-target-pathway network of top 20 pathways.

2.2.3. Cell cycle arrest assay

HCT116 cells (1×10^6/well) were spread in 6-well plates overnight; the cells were treated with different concentration of compound **5df** for 48 h. The cells were then washed twice with PBS and digested with trypsin. The supernatant was removed via centrifugation and fixed overnight in 70 % ethanol. The cells were washed twice with PBS and resuspended in a 190 μL staining buffer containing 4 μL of 1 mg/mL PI (propidium iodide), 4 μL of 10 mg/mL RNaseA (ribonuclease), and 0.2 μL Tritonx-100. After staining for 20 min in the dark, the cell cycle distribution was detected using flow cytometry (American BD,Canto II plus).

2.2.4. Cell apoptosis assay

HCT116 cells (2.2×10^6/well) were grown in 6-well plates and treated with different concentrations of compound **5df** for 48 h. After incubation, the cells were trypsinised and washed with PBS. The

Table 4

The twenty core targets of compound 5df against HCT116.

Target ID	Gene name	Degree	Betweenness	Closeness
AKT1	AKT Serine/Threonine Kinase 1	57	807.0940761	0.008695652
SRC	SRC Proto-Oncogene, Non-Receptor Tyrosine Kinase	50	470.9976093	0.008130081
EGFR	Epidermal Growth Factor Receptor	48	569.0928943	0.008064516
CASP3	Caspase 3	44	378.868961	0.007692308
ESR1	Estrogen Receptor 1	44	497.4969143	0.007633588
TNF	Tumor Necrosis Factor	43	470.5896637	0.007692308
MAPK1	Mitogen-Activated Protein Kinase 1	35	168.7924717	0.007092199
PIK3CA	Phosphatidylinositol-4,5-Bisphosphate 3-Kinase Catalytic Subunit Alpha	35	150.0517497	0.006944444
SIRT1	Sirtuin 1	34	221.1860693	0.007142857
MDM2	MDM2 Proto-Oncogene	34	265.0791359	0.006993007
CDC42	Cell Division Cycle 42	33	250.7977111	0.006849315
MMP9	Matrix Metallopeptidase 9	31	233.3490098	0.006944444
HDAC1	Histone Deacetylase 1	29	265.6142845	0.006578947
RPS6KB1	Ribosomal Protein S6 Kinase B1	28	100.9209659	0.006756757
CDK2	Cyclin Dependent Kinase 2	26	130.9764011	0.006578947
MMP2	Matrix Metallopeptidase 2	25	127.7503376	0.006578947
RAC1	Rac Family Small GTPase 1	24	107.5536357	0.00617284
PPARA	Peroxisome Proliferator Activated Receptor Alpha	22	366.0219331	0.006329114
PTPN1	Protein Tyrosine Phosphatase Non-Receptor Type 1	20	200.0227838	0.00617284
HMOX1	Heme Oxygenase 1	18	224.9469155	0.006134969

obtained cell pellet was resuspended in 1x Annexin binding buffer. 5 μL of annexin V/FITC and 10 μL of PI were added to the resuspended cells and incubated for 15 min at room temperature. Thereafter, the stained cells were analyzed by flow cytometry.

2.3. Analysis of network pharmacology

2.3.1. Prediction of disease targets of compound 5df

Compound **5df** was draw in ChemBioDraw and saved as "sdf" file format. This file was then imported into PharmMapper database (https://lilab-ecust.cn/pharmmapper/submitfile.html) (Wang et al., 2016), Swiss target prediction database (https://www.swisstargetprediction.ch) (Gfeller et al., 2013), inputting the protein names with the species limited to "Homo sapiens", and we could receive their official symbol. After these operations, proteins information of compound targets and known targets was obtained.

2.3.2. Gene screening of HCT116 related targets

Using "HCT116" as the search keywords, we searched Gene Cards database (https://www.genecards.org/) (Stelzer et al., 2016) to excavate potential targets associated with HCT116. Venny 2.1.0 (https://bioinfogp.cnb.csic.es/tools/venny/) software was used to identify the targets of compound **5df** against HCT116 (Sun et al., 2019).

2.3.3. Construction of protein–protein interaction (PPI) network

To further identify the core regulatory targets, PPI analysis was performed by submitting overlapping targets of active compounds in HCT116 to the STRING 11.5 database (https://string-db.org) (Szklarczyk et al., 2019). The species type was set to "Homo sapiens", the minimum interaction threshold was set to "highest confidence" > 0.4, and the rest was set as the default. Finally, the PPI result was imported into Cytoscape 3.8.0 software to construct a PPI network. Finally, the core targets of the top 20 were also exhibited.

2.3.4. Go and KEGG enrichment analysis

To further understand the functions of core target genes and the main action pathways of the active substances of **5df**, the disease-related targets obtained from the above screening were entered into the DAVID database (https://david.ncifcrf.gov/home.jsp) (Sherman et al., 2022). The list of genes of **5df** targets against HCT116 was uploaded to the DAVID searching tool. Here, the species section was selected as "homo sapiens", and all target gene names were corrected to their official names (official gene symbol), and the threshold of $p < 0.05$ was set for GO and KEGG enrichment before running the tool.

2.4. Molecular docking

Molecular docking was performed among the top three potential target proteins of HCT116 with **5df**. The 2D structure of compound **5df** was drawn by ChemDraw2019, and saved as cdx file. Then, MM2 force field was used to optimize the 3D structure of the ligand. The 3D structures of the target proteins were downloaded from the PDB database (https://www.rcsb.org) (AKT1, PDB: 3MV5; SRC, PDB: 1Y57; EGFR, PDB: 1 M17. The water molecules and the original ligands were removed from the target protein through Discovery studio. Later, the target proteins were imported into AutoDock Tools 1.5.6 for hydrogenation, charge calculation, and non-polar hydrogen combination, and then the result was stored in PDBQT format. The 3D coordinates of active sites (x, y, z) were as follows: AKT1 (1.931, −0.696, 25.291), SRC (9.48, 38.365, 38.325), EGFR (30.465, 9.823, 59.384). Finally, run AutoDock Tools 1.5.6 for molecular docking, and use Discovery studio 2021 to visualize the results (Trott & Olson, 2010).

2.5. Data analyses

The cell growth inhibition rate of compounds against six human cancer cell lines were calculated by the following formula: Inhibition rate (%) = (ODnegative control – ODexperiment)/(ODnegative control – ODblank) × 100 %. The relative cell viability was calculated with the formula: Cell viability rate (%) = (ODexperiment – ODblank)/(ODnegative control – ODblank) × 100 %. All data are expressed as mean ± SD, and each group was performed three times. Statistical analysis was processed by the SPSS 21.0 software (SPSS Inc., Chicago, USA).

3. Results and discussion

3.1. Chemistry

As illustrated in Scheme 1, the synthesis of the azophenol derivatives containing 1,3,4-oxadiazoles moiety was performed starting from the available chemicals. Firstly, according to the method we reported, a nucleophilic addition and elimination reaction between o-nitrobenzaldehyde and substituted hydrazides yielded acylhydrazone intermediates (**2aa ~ eg**) in the presence of acetic acid. Subsequently, these intermediates underwent a ring-closing reaction facilitated by iodine to form 1,3,4-oxadiazoles (**3aa ~ eg**) (Yu et al., 2021). In the subsequent step, the corresponding oxadiazoles were reacted with hydrated tin(II) chloride to yield intermediates **4aa ~ eg**, with yields ranging from 48 % to 93 %. Finally, compounds **4aa ~ eg** reacted with sodium nitrite to produce diazonium salts, which were further reacted with phenol to give azophenol derivatives containing the 1,3,4-oxadiazoles moiety (**5aa ~ eg**) in moderate to good yields (Table 1).

The structural characterization of all synthesized compounds was carried out using ¹H NMR, ¹³C NMR and HRMS (**see Supplementary Materials**). For example, the ¹H NMR spectrum of **5af** showed a single
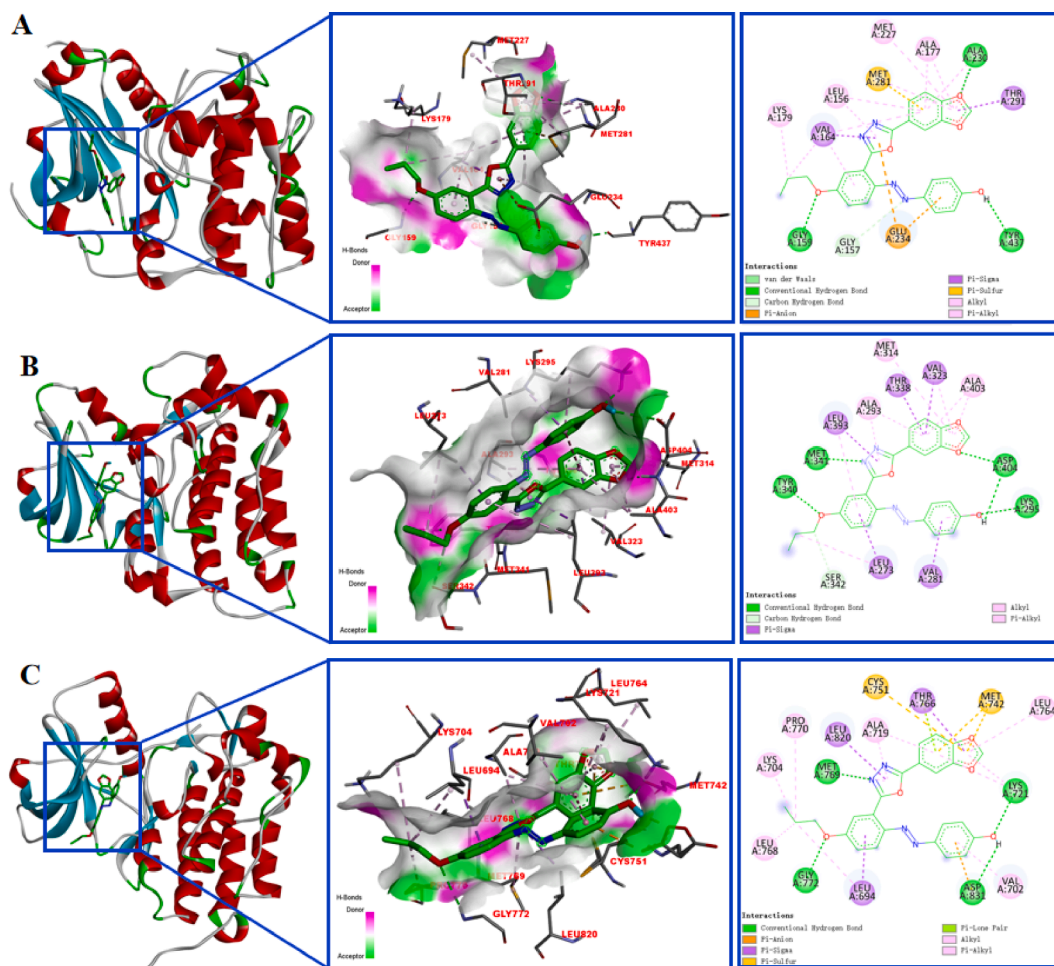
Fig. 6. Molecular models of **5df** binding to AKT1 (**A**), SRC (**B**), and EGFR (**C**).

peak at 10.45 ppm which could be assigned to –OH. two double peaks at 7.83 ppm (d, $J = 8.7$ Hz, 2H) and 6.95 ppm (d, $J = 8.8$ Hz, 2H) were attributed to the protons of phenol. The other a single peak at 7.45 ppm and two double peaks at 7.57 (d, $J = 8.1$ Hz, 1H) and 7.13 (d, $J = 8.1$ Hz, 1H) ppm belonged to the protons of benzo[d][1,3]dioxole. The single peaks of OCH$_2$O protons of benzo[d][1,3]dioxole moiety appeared at 6.18 ppm. In the ^{13}C NMR spectrum of **5af**, the signals at 164.5 and 162.9 ppm were assigned to the carbons in 1,3,4-oxadiazole. The carbon linked to hydroxyl groups appeared at 161.6 ppm. The signals at 125.5 and 116.0 ppm were assigned to the carbons of phenol. The single peaks at 102.1 ppm belonged to OCH$_2$O. The remaining multiple single peaks observed at 150.5–106.2 ppm were attributed to aromatic rings. The HRMS spectrum of **5af** showed a molecular ion peak at m/z 409.0907 as [M + Na]$^+$.

3.2. Biology assays

3.2.1. In vitro anticancer activity

The synthesized azophenol derivatives (**5aa ~ eg**) were assessed for their *in vitro* anticancer activities at 200 μmol/L against six human cancer cell lines, which included lung cancer cells (A549), cervical carcinoma cells (HeLa), colon cancer cells (HCT116), hepatocellular carcinoma cells (HePG2), breast cancer cells (MCF-7), and fibrosarcoma cells (HT1080). The MTT assay was used for this evaluation, and 5-fluorouracil (**5-Fu**) served as the positive control. As indicated in Table 2, most of the target compounds displayed significant anticancer activity, particularly against HCT116 and HePG2. For instance, compounds **5be**, **5cb**, **5db**, **5dc**, **5df**, **5ec** and **5eg** exhibited potent cytotoxicity against HCT116 and HePG2, with growth inhibition rates exceeding 60 %. Besides, **5db**, **5dc**, **5df** and **5ec** also demonstrated noteworthy cytotoxicity against HeLa, with growth inhibition rates of 85.81 %, 88.68 %, 78.87 %, and 80.13 %, respectively. Of particular note, compound **5df** exhibited substantial antineoplastic activity across all six tumor cell lines, with growth inhibition rates surpassing 50 %. These results underscored the potent anticancer effects of azophenol derivatives containing the 1,3,4-oxadiazoles moiety. Furthermore, preliminary structure–activity relationship (SAR) studies were also conducted. For example, to HCT116 and HePG2 cells, introduction of ethoxy or propoxy groups on R^2 led to more potent compounds (**5ca**, **5da** *vs* **5aa**). When R^1 was a ethoxy group, the compound **5be** with R^2 = (4-F)Ph exhibited superior anticancer activity compared to other 4-substituted phenyl variations. Similarly, when R^1 was a propoxy group, compounds **5cb** and **5df**, with the introduction of (4-F)Ph or benzo[d][1,3]dioxole groups on R^2 displayed more potent antitumor activity. On the contrary, introducing pyridine heterocycles in R^2 did not improve the activity of the compounds, such as **5ag**, **5bg**, **5cg**. This outcome indicated that the rational incorporation of propoxy group on R^1 and benzo[d][1,3]dioxole group on R^2 can distinct influence the anticancer effect.

Additionally, the IC$_{50}$ values (50 % inhibitory concentrations) of the tested compounds, where growth inhibition rates were over 70 %, were evaluated and consolidated in Table 3. Among these derivatives, the IC$_{50}$ values of **5db** and **5df** against HCT116 were measured at 9.96 and 4.09 μM, respectively. For HePG2 cells, the IC$_{50}$ value of **5dc** was determined to be 9.39 μM. These values are in close proximity to or even surpass the IC$_{50}$ of **5-FU**, the utilized positive control. In order to evaluate the safety of these new synthetic compounds, we selected the most active

compound **5df** and tested tis toxicity to human normal lung epithelial cells (BEAS-2B). The result showed that **5df** displayed low cytotoxicity against BEAS-2B with the cell viabilities over 80 % even at concentration of 160 μM, which indicated that compound **5df** showed higher selectivity to tumor cells than normal cells (Fig. 2).

3.2.2. Cell cycle analysis

Motivated by the initial *in vitro* antiproliferative screening outcomes, the underlying anticancer mechanism of this series compounds was further explored. Among the compounds, the most potent candidate, **5df**, was chosen to delve into its impact on the cell cycle progression of HCT116 cancer cells, employing flow cytometry analysis. For this investigation, HCT116 cancer cells were subjected to treatment with either DMSO (control group) or varying concentrations of **5df** (10, 20, 40 μM) for a duration of 48 h. As depicted in Fig. 3, the percentage of cells in the S phase in presence of **5df** exhibited values of 50.3 %, 52.8 %, and 59.0 %, respectively, while 26.7 % of the S phase was detected for the control group. These finding demonstrated that compound **5df** elicited a noticeable concentration-dependent S-phase arrest.

3.2.3. Cell apoptosis analysis

Moreover, cell apoptosis analysis was conducted on HCT116 cells exposed to escalating concentrations of 5df (0, 10, 20, 40 μM), utilizing the annexin V-FITC-PI assay. As illustrated in Fig. 4, following a 48-hour incubation period with **5df**, the collective percentages of late (Q2) and early (Q3) apoptotic cells exhibited increases to 17.5 %, 18.1 %, and 26.0 %, respectively. In contrast, the control group displayed a mere 3.0 % of apoptotic cells. Consequently, these results demonstrated that compound **5df** had antiproliferative activity through dose-dependently inducing cellular apoptosis.

3.3. Analysis of network pharmacology

Network pharmacology, an emerging discipline centered around the interplay of disease-gene-drug targets, has evolved into an efficacious research methodology for exploring active compounds and comprehending the mechanisms underlying the pharmacodynamic actions of these compounds (Hopkins, 2008; Zhu et al., 2022). In the context of this study, the network pharmacology approach was employed to uncover the mechanism of action and potential targets associated with compound **5df** in its application for HCT116 treatment.

As illustrated in Fig. 5, by searching the public databases (Swiss target prediction, PharmMapper, Gene Cards), confining the result to "Homo sapiens", 378 targets related with compound **5df** and 5412 targets with HCT116 were collected, respectively. The utilization of Venny 2.1.0 facilitated the calculation of the intersection between **5df** targets and HCT116 targets, resulting in 86 intersection targets (Fig. 5, **A**). Subsequently, high-confidence protein interaction data were extracted by employing target proteins and their corresponding components from the STRING database. This process eliminated uninvolved proteins, thereby yielding 86 shared proteins between **5df** and HCT116 (Fig. 5, **B**). The obtained protein–protein interaction (PPI) outcomes were imported into Cytoscape 3.8.0 software, enabling the construction of a PPI network (Fig. 5, **C**). The visualization also highlighted the twenty core targets. Notably, the top three targets, AKT serine/threonine kinase 1 (AKT1), SRC proto-oncogene, non-receptor tyrosine kinase (SRC), and epidermal growth factor receptor (EGFR), emerged as the most plausible targets of action for compound **5df** (Table 4). AKT1 belongs to a family of kinases AKT1, AKT2, AKT3, can include the coexpression of multiple family members in normal tissues and tumors. AKT is part of the PI3K/AKT pathway that encompasses multiple receptor tyrosine kinases (PI3K and mTOR) and integrates extracellular signals with cell growth, proliferation, and survival. It is often activated in malignant cells, and is a promising point of therapeutic intervention for many cancers (Nicholson and Anderson, 2002; Cheng et al. 2005). SRC kinase is a group of proteins with tyrosine protein kinase activity that are overexpressed and

highly activated in various human tumor cells, it can activate the MAPK and PI3K/Akt pathways related to tumor growth (Boggon and Eck, 2004; Peiró et al., 2014). EGFR is a member of the epidermal growth factor receptor (HER) family, widely distributed on the surface of mammalian epithelial cells, fibroblasts, glial cells, keratinocytes, and other cells. The EGFR signaling pathway plays an important role in physiological processes such as cell growth, proliferation, and differentiation. When EGFR undergoes mutations, it leads to sustained activation of the EGFR signaling pathway, leading to abnormal cell proliferation (Sabbah et al., 2020). The above three proteins were closely related to the development of tumor cells and might be the main targets of compound **5df**.

GO enrichment analysis and KEGG pathway enrichment analysis were also executed to shed light on the functions and enriched pathways attributed to the potential HCT116 genes targeted by compound **5df**. The analysis of biological processes (BP) outcomes indicated that compound **5df**'s targets involved in anti-HCT116 were prominently enriched in processes such as protein phosphorylation, protein autophosphorylation, negative regulation of the apoptotic process, and other biological processes. Cellular components (CC) analysis underscored the significance of cellular elements like cytosol, cytoplasm, nucleoplasm, and other cellular components. The molecular functions (MF) analysis results underscored that protein serine/threonine/tyrosine kinase activity, ATP binding, protein serine/threonine kinase activity and other molecular functions played an important role (Fig. 5, **D**). The KEGG pathway enrichment analysis yielded a notable result, 136 signaling pathways relevant to the interaction between **5df** and HCT116, were statistically significant. These included pathways associated with pathways in cancer, proteoglycans in cancer, prostate cancer, ErbB signaling pathway, and more. A visual representation in the form of a bubble diagram depicted the top 20 pathways which were significant enrichment potential, along with the highest count of associated genes (Fig. 5, **E**). Furthermore, a network was constructed to depict the relationships between ingredients, targets, and the top 20 pathways (Fig. 5, **F**). Among the pathways with the highest counts, such as pathways in cancer, proteoglycans in cancer, and prostate cancer, may contribute to the anti-HCT116 effect exhibited by **5df**.

3.4. Molecular docking

Molecular docking is a cutting-edge scientific method that can match small molecules to the binding sites of proteins and evaluate their binding strength to predict the binding mode and binding free energy of a given protein and small molecule ligand, and then study their function and mechanism of action (Kitchen et al., 2004; Saikia and Bordoloi, 2019). In recent years, molecular docking has played an important role in the validation of drug targets, and provided effective tools for the development of novel anticancer drugs (Premkumar et al., 2016; Shaheen et al., 2020; Eze et al., 2022). In this work, molecular docking studies were conducted between the compound **5df** and the three key targets, AKT1 (PDB: 3MV5), SRC (PDB: 1Y57), and EGFR (PDB: 1 M17) which were high-degree nodes in the interaction network to verify the results of network pharmacology analysis. The docking results showed that compound **5df** could be bound into the docking pockets with binding energies lower than −8 kcal/mol, and had good docking activities between the target proteins, suggesting they played a critical role in the response to compound **5df** in HCT116. For example, compound **5df** bound to AKT1 by forming hydrogen bonds with GLY159, ALA230, TYR437 (Fig. 6, **A**), which had the same binding sites and similar binding patterns as the AKT1 inhibitors that Freeman-Cook reported (Freeman-Cook et al., 2010). As shown in Fig. 6, **B**, Cowan-Jacob et al. demonstrated that the binding site of RSC inhibitors is composed of amino acid residues GLY274, LEU273, MET341, ALA293, LEU393, VAL281, GLN275 etc, by cultivating protein and drug complexes (Cowan-Jacob et al., 2005). There were also four hydrogen bonds, LYS295, TYR340, MET341 and ASP404 formed between **5df** and SRC,

indicates that the compound could bind to the active site of RSC. Similarly, compound **5df** was predicted to dock into the binding pocket of EGFR via hydrogen bonds LYS721, MET769, GLY772 and ASP831 (Fig. 6, **C**), which was the active site of EGFR (Stamos et al., 2002). The above data suggested that compound **5df** could potentially influence their function by inhibiting the binding of the docking pockets to the target receptors and played an crucial role in anti-HCT116.

4. Conclusion

In summary, this study encompassed the synthesis of thirty-five azophenol derivatives containing the 1,3,4-oxadiazoles moiety, whose structures were elucidated through ^{1}H NMR, ^{13}C NMR and HRMS analyses. The anticancer activity of all synthesized compounds was evaluated *in vitro* against six different human cancer cell lines via the MTT assay. Remarkably, compound **5df** exhibited a notable inhibition of HCT116 cell proliferation with an IC$_{50}$ value of 4.09 ± 0.04 μM, and low toxicity against normal human cells. Further mechanism studies showed that **5df** significantly arrested cell cycle at S phase, induced apoptosis via flow cytometric analysis. In addition, network pharmacology computations pointed towards AKT1, SRC, and EGFR as plausible target proteins for **5df** against HCT116 cells. Molecular docking studies further confirmed the good binding interactions of **5df** with these three target proteins. Collectively, these results demonstrated that compound **5df** could be a potent anticancer candidate reagent with low toxicity, and worthy for further investigation.

Declaration of Competing Interest

The authors declare that they have no known competing financial interests or personal relationships that could have appeared to influence the work reported in this paper.

Acknowledgements

Appendix A. Supplementary material

Supplementary data to this article can be found online at https://doi.org/10.1016/j.arabjc.2023.105386.

References

Abd-Ellah, H.S., Abdel-Aziz, M., Shoman, M.E., Beshr, E.A.M., Kaoud, T., Ahmed, A.F.F., 2017. New 1,3,4-oxadiazole/oxime hybrids: design, synthesis, anti-inflammatory, COX inhibitory activities and ulcerogenic liability. Bioorg. Chem. 74, 15–29. https://doi.org/10.1016/j.bioorg.2017.06.003.

Abou-Seri, S.M., 2010. Synthesis and biological evaluation of novel 2,4'-bis substituted diphenylamines as anticancer agents and potential epidermal growth factor receptor tyrosine kinase inhibitors. Eur. J. Med. Chem. 45 (9), 4113–4121. https://doi.org/10.1016/j.ejmech.2010.05.072.

Ahsan, M.J., Samy, J.G., Khalilullah, H., Nomani, M.S., Saraswat, P., Gaur, R., Singh, A., 2011. Molecular properties prediction and synthesis of novel 1,3,4-oxadiazole analogues as potent antimicrobial and antitubercular agents. Bioorg. Med. Chem. Lett. 21 (24), 7246–7250. https://doi.org/10.1016/j.bmcl.2011.10.057.

Andreani, A., Granaiola, M., Leoni, A., Morigi, R., Ramballdi, M., 2001. Synthesis and antitubercular activity of imidazo [2,1-b]thiazoles. Eur. J. Med. Chem. 36, 743–746. https://doi.org/10.1016/S0223-5234(01)01266-1.

Atay, Ç.K., Gökalp, M., Tuncer, B.Ö., Tilki, T., 2017. Antimicrobial activities and absorption properties of disazo dyes containing imidazole and pyrazole moieties. J. Macromol. Sci., Part A Pure Appl. Chem. 54 (4), 236–242. https://doi.org/10.1080/10601325.2017.1282695.

Bajaj, S., Asati, V., Singh, J., Roy, P.P., 2015. 1,3,4-Oxadiazoles: an emerging scaffold to target growth factors, enzymes and kinases as anticancer agents. Eur. J. Med. Chem. 97, 124–141. https://doi.org/10.1016/j.ejmech.2015.04.051.

Benkhaya, S., M'rabet, S., El Harfi, A., 2020. Classifications, properties, recent synthesis and applications of azo dyes. Heliyon 6 (1), e03271.

Boggon, T.J., Eck, M.J., 2004. Structure and regulation of Src family kinases. Oncogene 23 (48), 7918–7927. https://doi.org/10.1038/sj.onc.1208081.

Bray, F., Ferlay, J., Soerjomataram, I., Siegel, R.L., Torre, L.A., Jemal, A., 2018. Global cancer statistics 2018: GLOBOCAN estimates of incidence and mortality worldwide for 36 cancers in 185 countries. CA Cancer J. Clin. 68 (6), 394–424. https://doi.org/10.3322/caac.21492.

Cheng, J.Q., Lindsley, C.W., Cheng, G.Z., Yang, H., Nicosia, S.V., 2005. The Akt/PKB pathway: molecular target for cancer drug discovery. Oncogene 24 (50), 7482–7492. https://doi.org/10.1038/sj.onc.1209088.

Cowan-Jacob, S.W., Fendrich, G., Manley, P.W., Jahnke, W., Fabbro, D., Liebetanz, J., Meyer, T., 2005. The crystal structure of a c-Src complex in an active conformation suggests possible steps in c-Src activation. Structure 13 (6), 861–871. https://doi.org/10.1016/j.str.2005.03.012.

Eze, C.C., Ezeokonkwo, A.M., Ugwu, I.D., Eze, U.F., Onyeyilim, E.L., Attah, I.S., Okonkwo, I.V., 2022. Azole-pyrimidine hybrid anticancer agents: a review of molecular structure, structure activity relationship, and molecular docking. Anticancer Agents Med. Chem. 22 (16), 2822–2851. https://doi.org/10.2174/1871520622666220318090147.

Freeman-Cook, K.D., Autry, C., Borzillo, G., Gordon, D., Barbacci-Tobin, E., Bernardo, V., Briere, D., Clark, T., Corbett, M., Jakubczak, J., Kakar, S., Knauth, E., Lippa, B., Luzzio, M.J., Mansour, M., Martinelli, G., Marx, M., Nelson, K., Pandit, J., Rajamohan, F., Robinson, S., Subramanyam, C., Wei, L., Wythes, M., Morris, J., 2010. Design of selective, ATP-competitive inhibitors of Akt. J. Med. Chem. 53 (12), 4615–4622. https://doi.org/10.1021/jm1003842.

Gfeller, D., Michielin, O., Zoete, V., 2013. Shaping the interaction landscape of bioactive molecules. Bioinformatics 29 (23), 3073–3079. https://doi.org/10.1093/bioinformatics/btt540.

Guo, Y., Xu, T., Bao, C., Liu, Z., Fan, J., Yang, R., Qin, S., 2019. Design and synthesis of new norfloxacin-1,3,4-oxadiazole hybrids as antibacterial agents against methicillin-resistant Staphylococcus aureus (MRSA). Eur. J. Pharm. Sci. 136, 104966 https://doi.org/10.1016/j.ejps.2019.104966.

Harfenist, M., Heuser, D.J., Joyner, C.T., Batchelor, J.F., White, H.L., 1996. Selective inhibitors of monoamine oxidase. 3. Structure-activity relationship of tricyclics bearing imidazoline, oxadiazole, or tetrazole groups. J. Med. Chem. 39 (9), 1857–1863. https://doi.org/10.1021/jm950595m.

Hopkins, A.L., 2008. Network pharmacology: the next paradigm in drug discovery. Nat. Chem. Biol. 4 (11), 682–690. https://doi.org/10.1038/nchembio.118.

Kitchen, D.B., Decornez, H., Furr, J.R., Bajorath, J., 2004. Docking and scoring in virtual screening for drug discovery: methods and applications. Nat. Rev. Drug Discov. 3 (11), 935–949. https://doi.org/10.1038/nrd1549.

Maliyappa, M.R., Keshavayya, J., Mallikarjuna, N.M., Pushpavathi, I., 2020. Novel substituted aniline based heterocyclic dispersed azo dyes coupling with 5-methyl-2-(6-methyl-1, 3-benzothiazol-2-yl)-2, 4-dihydro-3*H*-pyrazol-3-one: synthesis, structural, computational and biological studies. J. Mol. Struct. 1205, 127576 https://doi.org/10.1016/j.molstruc.2019.127576.

Manjunatha, B., Bodke, Y.D., 2021. Novel isoxazolone based azo dyes: synthesis, characterization, computational, solvatochromic UV-Vis absorption and biological studies. J. Mol. Struct. 1244, 130933 https://doi.org/10.1016/j.molstruc.2021.130933.

Manjunatha, B., Bodke, Y.D., Nagaraja, O., Nagaraju, G., Sridhar, M.A., 2021. Coumarin-benzothiazole based azo dyes: synthesis, characterization, computational, photophysical and biological studies. J. Mol. Struct. 1246, 131170 https://doi.org/10.1016/j.molstruc.2021.131170.

Matada, M.N., Jathi, K., Rangappa, M.M., Geoffry, K., Kumar, S.R., Nagarajappa, R.B., Zahara, F.N., 2020. A new sulphur containing heterocycles having azo linkage: synthesis, structural characterization and biological evaluation. J. King Saud Univ. Sci. 32 (8), 3313–3320. https://doi.org/10.1016/j.jksus.2020.09.016.

Mohammadi, A., Khalili, B., Tahavor, M., 2015. Novel push-pull heterocyclic azo disperse dyes containing piperazine moiety: Synthesis, spectral properties, antioxidant activity and dyeing performance on polyester fibers. Spectrochim. Acta A Mol. Biomol. Spectrosc. 150, 799–805. https://doi.org/10.1016/j.saa.2015.06.024.

Nicholson, K.M., Anderson, N.G., 2002. The protein kinase B/Akt signalling pathway in human malignancy. Cell. Signal. 14 (5), 381–395. https://doi.org/10.1016/S0898-6568(01)00271-6.

Peiró, G., Ortiz-Martínez, F., Gallardo, A., Pérez-Balaguer, A., Sánchez-Payá, J., Ponce, J. J., Tibau, A., López-Vilaro, L., Escuin, D., Adrover, E., Barnadas, A., Lerma, E., 2014. Src, a potential target for overcoming trastuzumab resistance in HER2-positive breast carcinoma. Br. J. Cancer 111 (4), 689–695. https://doi.org/10.1038/bjc.2014.327.

Peng, L., Weigl, K., Boakye, D., Brenner, H., 2018. Risk scores for predicting advanced colorectal neoplasia in the average-risk population: a systematic review and meta-analysis. Am. J. Gastroenterol. 113 (12), 1788–1800. https://doi.org/10.1038/s41395-018-0209-2.

Premkumar, S., Rekha, T.N., Mohamed Asath, R., Mathavan, T., Milton Franklin Benial, A., 2016. Vibrational spectroscopic, molecular docking and density functional theory studies on 2-acetylamino-5-bromo-6-methylpyridine. Eur. J. Pharm. Sci. 82, 115–125. https://doi.org/10.1016/j.ejps.2015.11.018.

Ravi, B.N., Keshavayya, J., Mallikarjuna, N.M., Santhosh, H.M., 2020. Synthesis, characterization, cyclic voltammetric and cytotoxic studies of azo dyes containing thiazole moiety. Chem. Data Collect. 25, 100334 https://doi.org/10.1016/j.cdc.2019.100334.

Sabbah, D.A., Hajjo, R., Sweidan, K., 2020. Review on epidermal growth factor receptor (EGFR) structure, signaling pathways, interactions, and recent updates of EGFR inhibitors. Curr. Top. Med. Chem. 20 (10), 815–834. https://doi.org/10.2174/1568026620666200303123102.

Saikia, S., Bordoloi, M., 2019. Molecular docking: challenges, advances and its use in drug discovery perspective. Curr. Drug Targets 20 (5), 501–521. https://doi.org/10.2174/1389450119666181022153016.

Sawicki, T., Ruszkowska, M., Danielewicz, A., Niedźwiedzka, E., Arłukowicz, T., Przybyłowicz, K.E., 2021. A review of colorectal cancer in terms of epidemiology, risk factors, development, symptoms and diagnosis. Cancers (basel). 13 (9), 2025. https://doi.org/10.3390/cancers13092025.

Shaheen, M.A., El-Emam, A.A., El-Gohary, N.S., 2020. Design, synthesis and biological evaluation of new series of hexahydroquinoline and fused quinoline derivatives as potent inhibitors of wild-type EGFR and mutant EGFR (L858R and T790M). Bioorg. Chem. 105, 104274 https://doi.org/10.1016/j.bioorg.2020.104274.

Shen, T., Cai, L.D., Liu, Y.H., Li, S., Gan, W.J., Li, X.M., Wang, J.R., Guo, P.D., Zhou, Q., Lu, X.X., Sun, L.N., Li, J.M., 2018. Ube2v1-mediated ubiquitination and degradation of Sirt1 promotes metastasis of colorectal cancer by epigenetically suppressing autophagy. J. Hematol. Oncol. 11 (1), 95. https://doi.org/10.1186/s13045-018-0638-9.

Sherman, B.T., Hao, M., Qiu, J., Jiao, X., Baseler, M.W., Lane, H.C., Imamichi, T., Chang, W., 2022. DAVID: a web server for functional enrichment analysis and functional annotation of gene lists (2021 update). Nucleic Acids Res. 50 (W1), W216–W221. https://doi.org/10.1093/nar/gkac194.

Shingalapur, R.V., Hosamani, K.M., Keri, R.S., Hugar, M.H., 2010. Derivatives of benzimidazole pharmacophore: synthesis, anticonvulsant, antidiabetic and DNA cleavage studies. Eur. J. Med. Chem. 45 (5), 1753–1759. https://doi.org/10.1016/j.ejmech.2010.01.007.

Stamos, J., Sliwkowski, M.X., Eigenbrot, C., 2002. Structure of the epidermal growth factor receptor kinase domain alone and in complex with a 4-anilinoquinazoline inhibitor. J. Biol. Chem. 277 (48), 46265–46272. https://doi.org/10.1074/jbc.M207135200.

Stelzer, G., Rosen, N., Plaschkes, I., Zimmerman, S., Twik, M., Fishilevich, S., Stein, T.I., Nudel, R., Lieder, I., Mazor, Y., Kaplan, S., Dahary, D., Warshawsky, D., Guan-Golan, Y., Kohn, A., Rappaport, N., Safran, M., Lancet, D., 2016. The genecards suite: from gene data mining to disease genome sequence analyses. Curr. Protoc. Bioinformatics 54.

Sun, L., Dong, S., Ge, Y., Fonseca, J.P., Robinson, Z.T., Mysore, K.S., Mehta, P., 2019. DiVenn: an interactive and integrated web-based visualization tool for comparing gene lists. Front. Genet. 10, 421. https://doi.org/10.3389/fgene.2019.00421.

Sung, H., Ferlay, J., Siegel, R.L., Laversanne, M., Soerjomataram, I., Jemal, A., Bray, F., 2011. Global cancer statistics 2020: GLOBOCAN estimates of incidence and mortality worldwide for 36 cancers in 185 countries. CA Cancer J. Clin. 71 (3), 209–249. https://doi.org/10.3322/caac.21660.

Szklarczyk, D., Gable, A.L., Lyon, D., Junge, A., Wyder, S., Huerta-Cepas, J., Simonovic, M., Doncheva, N.T., Morris, J.H., Bork, P., Jensen, L.J., Mering, C.V., 2019. STRING v11: protein-protein association networks with increased coverage, supporting functional discovery in genome-wide experimental datasets. Nucleic Acids Res. 47 (D1), D607–D613. https://doi.org/10.1093/nar/gky1131.

Tahir, T., Ashfaq, M., Saleem, M., Rafiq, M., Shahzad, M.I., Mojzych, M., Kotwica-Mojzych, K., 2021. Pyridine scaffolds, phenols and derivatives of azo moiety: current therapeutic perspectives. Molecules 26 (16), 4872. https://doi.org/10.3390/molecules26164872.

Trott, O., Olson, A.J., 2010. AutoDock Vina: improving the speed and accuracy of docking with a new scoring function, efficient optimization, and multithreading. J. Comput. Chem. 31 (2), 455–461. https://doi.org/10.1002/jcc.21334.

Wang, X., Pan, C., Gong, J., Liu, X., Li, H., 2016. Enhancing the enrichment of pharmacophore-based target prediction for the polypharmacological profiles of drugs. J. Chem. Inf. Model. 56 (6), 1175–1183. https://doi.org/10.1021/acs.jcim.5b00690.

Wang, X., Chai, J., Kong, X., Jin, F., Chen, M., Yang, C., Xue, W., 2021. Expedient discovery for novel antifungal leads: 1,3,4-Oxadiazole derivatives bearing a quinazolin-4(3H)-one fragment. Bioorg. Med. Chem. 45, 116330 https://doi.org/10.1016/j.bmc.2021.116330.

Woods, D., Turchi, J.J., 2013. Chemotherapy induced DNA damage response: convergence of drugs and pathways. Cancer Biol. Ther. 14 (5), 379–389. https://doi.org/10.4161/cbt.23761.

Yu, X., Zhao, Y.F., Huang, G.J., Chen, Y.F., 2021. Design and synthesis of 7-diethyla-minocoumarin-based 1,3,4-oxadiazole derivatives with anti-acetylcholinesterase activities. J. Asian Nat. Prod. Res. 23 (9), 866–876. https://doi.org/10.1080/10286020.2020.1803293.

Yu, X., Xi, Y., Sui, Y., Liu, Y., Chen, G., Zhang, M., Zhang, Y., Luo, G., Long, Y., Yang, W., 2023. Hydroxide-Mediated SNAr rearrangement for synthesis of novel depside derivatives containing diaryl ether skeleton as antitumor agents. Molecules 28 (11), 4303. https://doi.org/10.3390/molecules28114303.

Zhang, X.M., Qiu, M., Sun, J., Zhang, Y.B., Yang, Y.S., Wang, X.L., Tang, J.F., Zhu, H.L., 2011. Synthesis, biological evaluation, and molecular docking studies of 1,3,4-oxadiazole derivatives possessing 1,4-benzodioxan moiety as potential anticancer agents. Bioorg. Med. Chem. 19 (21), 6518–6524. https://doi.org/10.1016/j.bmc.2011.08.013.

Zhu, W., Li, Y., Zhao, J., Wang, Y., Li, Y., Wang, Y., 2022. The mechanism of triptolide in the treatment of connective tissue disease-related interstitial lung disease based on network pharmacology and molecular docking. Ann. Med. 54 (1), 541–552. https://doi.org/10.1080/07853890.2022.2034931.